2013

Exploration of the Neurochemistry, Structural Morphology and Behavior in the GCPII+/- Mouse Model with Magnetic Resonance

Palig Mouradian
pmouradi@wellesley.edu

Exploration of the Neurochemistry, Structural Morphology and Behavior in the GCPII$^{+/-}$ Mouse Model with Magnetic Resonance

Palig Mouradian

Advisor: Nancy H. Kolodny

Department of Chemistry

Wellesley College

Submitted in Partial Fulfillment of the Prerequisite for Honors in Neuroscience

May 2013

Acknowledgments

I would first like to thank my advisor, Nancy H. Kolodny, for believing in me. She is responsible for cultivating my curiosity, introducing me to the excitement of scientific inquiry and ultimately, pushing me to believe in myself. Her support, guidance and shared enthusiasm made this project both possible and invaluable over the past 3 years.

I wish to also thank Laura Schaevitz who taught me so much over the past few years and who played a crucial role in the success of many of this project's components. A thanks to my thesis committee; Deborah Bauer and Mike Wiest for helping me brainstorm, and for reading my thesis. A special thanks to Brandon Abbs who voluntarily ensured the accuracy and breadth of my thesis. Thank you to former labmates who set amazing examples; Stephanie S. Huang and Weiya Mu as well as current labmates Tamara Biary and Heather Pearson who weathered the storm every step of the way and who played a large part in the success and completion of my project.

I also want to express my appreciation to Pat Carey and Val LePage for offering advice, aid and tending to the mice as well as Jon Rose for always fixing the NMR and being there for instrument and protocol needs as well as Joy Renjilian-Burgy for always looking out for me.

Thank you to my great friends who helped me from understanding basic computing to reinforcing my dedication and motivation for this project. In no particular order, Tanya Antounian, Anoush Youssoufian, Sima Lotfi, Elizabeth Exil, Zain Fanek, Laura Marin, Priscilla Galvan, Talar Keskinyan, Katie Hargreaves, Gina White, Rachel Parker, Blake Desormeaux, Naje Simama,Silvia Galis-Menendez, Stephanie Schmitt, Lina Torres, Rachel Cherny, Christianne Wolfsen and the rest of Punch's Alley pub staff past and present. A thanks to my Wellesley big sister, Adriane Otopalik and little sister, Joanna Milton. Thank you to my parents who let me talk about this at dinner while pretending to listen as well as my cousin, Talar Mouradian.

I would finally like to thank the following musicians/bands for making the writing of this thesis possible; The Cure, White Lies, Alkaline Trio, Yanni, and Stars.

Abstract

Schizophrenia plagues approximately 1% of the world's population. This chronic brain disorder is marked by behavioral, cognitive and social abnormalities. Studies on the brain pathophysiology of schizophrenia have also found predominant structural and neurochemical aberrations. While no single cause of the disorder has been identified; environmental, genetic and epigenetic factors have been implicated. This thesis is both an investigation of the genetically modified GCPII$^{+/-}$ mouse model as well as the groundwork for the implementation of diffusion tensor imaging and an updated epigenetic mouse model. Groundwork for the updated mouse model included rodent stereotactic surgery design to ultimately induce epigenetic dysregulation with hopes of better modeling the variable development and symptomology of schizophrenia. The primary GCPII$^{+/-}$ mouse model sustains decreased expression of the enzyme glutamate carboxypeptidase II (GCPII) integral for glutamate synthesis in order to diminish glutamatergic N-methyl-d-aspartate (NMDA) receptor activity. Magnetic resonance imaging, spectroscopy and a social task were used to test for the abnormalities that GCPII$^{+/-}$ might exhibit. Tests were conducted on both mice heterozygous for GCPII$^{+/-}$ mutation (HET) and their wild-type (WT) counterparts at numerous ages corresponding to mouse adolescence and adulthood. We hypothesized that HET mice would exhibit differential volume of brain structures and neurometabolites compared to WT mice, as well as social deficiency.

Magnetic resonance imaging (MRI) and spectroscopy (MRS) data were obtained on post natal days (PND) 35/36, 49/50 and 63/64 and social task data were obtained between PND 114 and 117. Both MRI and MRS data revealed sex differences. HET males exhibited more structural abnormalities than HET females with greater hippocampal asymmetry and decreased right hippocampal volume compared to WT males. Ventricular enlargement or asymmetry was not reported in HET males nor females. HET females exhibited more abnormalities in neurometabolite levels with elevated levels of choline and glutamate, as well as diminished levels of N-acetylaspartate and N-acetylaspartylglutamate compared to WT females. Behavioral data found that both HET males and females exhibit a social deficit. Each sets of results mirrored findings in MRI and MRS studies on schizophrenia as well as characteristic social abnormalities. Data serve as a testament to the promise of the GCPII$^{+/-}$ mouse model but are also indicative of the model's shortcomings.

Table of Contents

Introduction

Introduction to Schizophrenia

In 1972, Plum declared schizophrenia to be the "graveyard of neuropathologists" (Andreasen 2005). Such a characterization is fitting for a brain disorder with both a multitude of symptoms and a variety of potential causes. Approximately 1.1 % of the global population suffers from schizophrenia (SZ) and diagnosis is standardized by the American Psychological Association (APA) Diagnostic and Statistical Manual of Mental Disorders (DSM-IV) and by the International Classification of Diseases criteria (ICD-10) (Organization 2004; Association 2000). Both tools detail SZ as a heterogeneous disorder that manifests as several subtypes consisting of various sets of symptoms. Symptoms include delusions, hallucinations, disorganized speech, disorganized or catatonic behavior, flattened affect, speech deficit and avolition, as well as compromised independence, interpersonal relations and occupational status (Association 2000). Symptoms can be classified either as active-phase or negative. Active-phase symptoms can be considered positive symptoms as they are the presentation of abnormalities which include hallucinations (visual, auditory, olfactory, and somatosensory) and delusions as well as disorganized speech and catatonic behavior (Kay 2007). Negative symptoms are the absence of normal behaviors such as deficits in communication, avolition, and flattened affect. Those with SZ will also typically exhibit diminished working memory, difficulties in attention, compromised independence and occupational dysfunction (Kay 2007; Association 2000).

Onset of symptoms typically occurs during adolescence. Active phase or positive symptoms must be present for a month with or without negative symptoms prior to diagnosis and must not result from drug use or medical conditions.

Structural Abnormalities in SZ

These symptoms comprised much of the known psychopathology of SZ prior to the revolution of neuroimaging. Post mortem studies did not find conclusive data due to the inconsistencies present in the acquisition of tissues, clinical diagnoses and the more qualitative nature of the original exploration into structural abnormalities (Powchik et al. 1998). While postmortem studies have improved with more specific and advanced labeling methods as well as systematic tissue retrieval over the past two decades, they are still unable to assess functional abnormalities as well as alterations over time (Shenton et al. 2001). Computed Tomography (CT), Magnetic Resonance Imaging (MRI), and Diffusion Tensor Imaging (DTI) have emerged as non-invasive tools capable of discovering structural abnormalities previously too minute to elucidate. In 1976 Johnston et al.'s CT study definitively confirmed findings of enlarged lateral ventricles in SZ patients from pneumonencephalography and postmortem brain studies (Johnston et al. 1976).

Over the past three decades, MRI data have provided a vast amount of information on the structural abnormalities in the schizophrenic brain. Table 1 lists predominant findings from a recent review of neuroimaging studies and the associated pathology of specific structural abnormalities (Shenton 2010; Shenton 2010). Relevant brain structures and abnormalities are shown below the table (Fig.1.).

Table.1. Predominant structural abnormalities. Their prevalence and associated role in pathophysiology of schizophrenia (Shenton 2010).

Structure	Prevalence of Findings	Associated Pathology
Enlarged Lateral Ventricles	80%	Abnormal cerebral development and Necrosis
Enlarged Third Ventricles	73%	Abnormal development and neurodegeneration of thalamus
Reduced Amygdala	74%	Implicates pre and perinatal environmental assaults Diminished emotional expression Diminished memory encoding
Reduced Hippocampus and Parahippocampal gyrus	74%	Implicates pre and perinatal environmental assaults Diminished plasticity Impairments in cognition and memory
Reduced Superior temporal gyrus	67%	Auditory hallucinations Verbal memory deficits Thought disorder
Reduced Frontal Lobe	59%	Poor performance in Wisconsin Card Sorting Task Eye tracking abnormalities Spatial working memory deficits
Reduced Parietal Lobe	60%	Thought disorder Diminished attention Diminished spatial working memory Disturbed language ability
Cavum Septum Pellucidum	92%	Disrupted or asymmetric cerebral development
Enlarged Basal ganglia	68%	Attributed to drug treatment Abnormal cognitive, sensory and motor processing
Reduced Corpus Callosum	63%	Deficit in information processing Diminished interhemispheric communication
Thalamus	42%	Diminished attention and information processing Deficits in modulation of limbic system and cortical areas Regulates connections between cortex and cerebellum Cognitive dysmetria
Cerebellum	31%	Cognitive processing Regulation of cortical and limbic circuit interaction

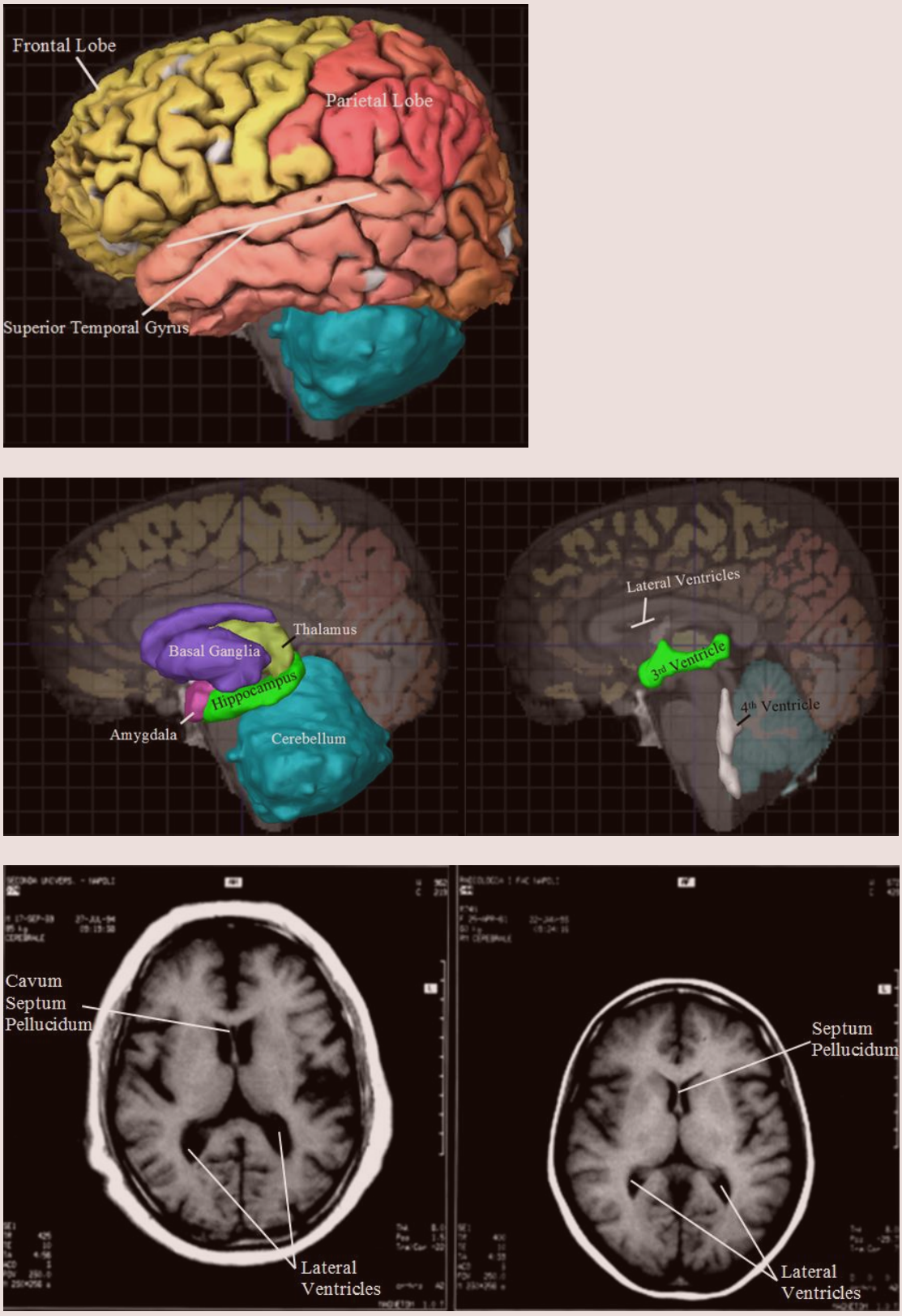

Fig. 1. Brain structures relevant to schizophrenia pathology. *Top* image identifies superior temporal gyrus, as well as frontal and temporal lobes. *Middle* image illustrates internal structures on left; thalamus, basal ganglia, amygdala, hippocampus, cerebellum and ventricles on right; 3rd, 4th, and lateral. *Bottom* image on left presents marker enlarged lateral ventricles and cavum septum pellucidum in schizophrenic brain compared to healthy brain on right (Galderisi et al. 2000). Allen Human Brain Atlas for 3-Dimensional rendering.

8

Such findings demonstrate the spectrum of brain phenomena observed in SZ. MRI data concentrated on volumetric differences in the gray matter of the brain and it was not until the application of Diffusion Tensor Imaging that interest grew in assessing white matter. The development of DTI in the late 1990s coincided with postmortem brain studies in the early 2000's, the latter of which observed abnormalities in glial cell development in SZ (Kubicki et al. 2005). A class of glial cells, oligodendrocytes, comprises the fatty myelin sheaths that cover axons. These myelin sheaths are crucial to normal signal propagation and sustaining connections among neurons. Demyelination is indicative of neuronal breakdown and death (Kubicki et al. 2005). In the brain, axons join together to form tracts and bundles.

Diffusion tensor imaging probes the structural integrity of white matter connections and tracts. DTI studies investigate aberrations in organization and viability of axons and the connections that they form. The majority of DTI studies have found abnormalities in a myriad of fiber tracts responsible for connections between and among the frontal and temporal lobes, that play roles in memory, learning, emotion, language, hallucinations as well as behavior.

CT, MRI and DTI greatly enabled researchers to explore structural abnormalities in the SZ brains but these means could not elucidate abnormalities in neural activity or neurochemistry. The advent of functional magnetic resonance imaging (fMRI) and magnetic resonance spectroscopy (MRS) offered the necessary tools for probing the SZ brain for such aberrations. Such tools mostly functioned to evaluate the hypotheses generated by the use of psychomimetic drugs.

Psychomimetic Drugs and SZ

The effects of drugs such as lysergic acid diethylamide (LSD), cocaine, ketamine, and phencyclidine (PCP) led to the pharmacologically informed hypotheses of abnormalities present in the SZ brain. LSD and cocaine mainly elicit positive symptoms of the disorder through their hallucinogenic effects in healthy users and exacerbation in those who already suffer from it (Crow 1980). Recently, the LSD mouse model was revisited as a means to explore SZ (Marone-Lewicka et al. 2011). This investigation was fueled by the dual effect of LSD that consists of both a hallucinogenic phase and a subsequent paranoid one. This study found that these effects of LSD are mediated by both serotonin receptor subtype 5HT2 activity and dopamine receptors D2 and D4. D2 receptors and 5HT2 receptors were found to have been upregulated and downregulated, respectively. Such findings are indicative of the agonistic effects of LSD on serotonergic and dopaminergic receptors and link hyperactive serotonergic and mesolimbic dopaminergic neurotransmission with symptoms of SZ.

On the other hand the dissociative anesthetics PCP and Ketamine elicit the positive, negative and cognitive symptoms characteristic of SZ (Morris et al. 2005). Both of these compounds antagonize N-methyl-d-aspartate receptors (NMDAR), one of the main ionotropic glutamate receptors in the central nervous system (CNS).

NMDA Receptors

NMDARs are ligand gated ion channels that can be found on both pre and post synaptic neurons and must be coactivated by both glutamate, the major excitatory neurotransmitter of the (CNS), and glycine or d-serine which are present at low levels in the synapse (Blanke and Vandongen 2009) (Fig. 2.). In addition, this coactivation must be

simultaneous with sufficient membrane depolarization or else the receptor cannot allow ions through. NMDA receptors consequently function as coincidence detectors of glutamate release and membrane depolarization, the basis for their role in Hebbian synaptic plasticity. They are crucial for a number of other processes that occur throughout the development and maturation of the CNS as well, including synaptic transmission, learning and memory and structural modifications of dendrites and dendritic spines (Blanke and Vandongen 2009).

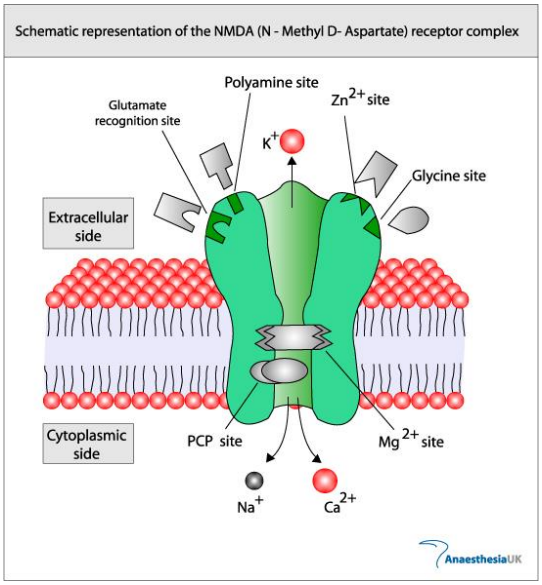

Fig. 2. NMDA receptor complex. Phencyclidine (PCP) is a dissociative anesthetic. Potassium ions (K^+), sodium ions (Na^+) and calcium ions (Ca^{2+}) flow through ion channel. (AnaesthesiaUK).

The effects of PCP and Ketamine implicated NMDAR hypofunction in the symptomology of SZ and various phenomena of the disorder. Such phenomena include reduced spine densities and compromised dendritic structure in cortical glutamatergic neurons (Glantz and Lewis 2000) as well as disrupted parvalbumin positive (PV) GABAergic interneurons in cortico-limbic and hippocampal neural circuits (Nakazawa et al. 2012). In healthy brains, dendrites and spine densities are crucial arenas for learning

and memory (Lee et al. 2012). NMDA receptors are found on spines and allow for independent action potentials within the dendrites (Blanke and Vandogen 2009) leading to strengthened structures and increased spine density. It is hypothesized that the hypoactivity of these receptors, as in SZ, will result in reduced spine density and deteriorated integrity of these structures.

NMDA receptors are the primary form of excitatory input for GABAergic interneurons, thereby establishing the relevance of these interneurons. PV GABAergic interneurons of the hippocampus are a subset of GABAergic interneurons which have been shown to be significantly more sensitive to NMDAR antagonism than pyramidal neurons (Grunze et al. 1996). Disrupted gamma oscillations and cognitive and behavioral defects in SZ are taken as evidence for asynchronous neuronal circuits. Nakazawa and his colleagues argue that NMDAR hypofunction impairs the fast-spiking neurons responsible for neural synchrony. Fast-spiking neurons are mostly comprised of PV GABAergic interneurons, which modulate and synchronize neural activity within cortical and hippocampal neural circuits by balancing excitation with inhibition. They play major roles in the proper maturation and development of these circuits. These interneurons are responsible for the inhibition of subcortical dopaminergic neurons as well as neurons within the hippocampus which have been shown to be hyperactive in SZ (Nakazawa et al. 2012, Grunze et al. 1996)

The role of GABAergic interneurons in SZ is further bolstered by evidence that NMDAR antagonists, such as ketamine and PCP, decrease levels of the GABA synthesizing enzyme, glutamic acid decarboxylase 67 (gad67) and parvalbumin (PV) in cortical GABAergic neurons (Nakazawa et al. 2012) and diminish inhibitory input onto

pyramidal neurons (Coyle 2012). These findings inextricably link hypofunction of NMDA receptors with a predominant pathology of SZ. The reduction of gad67 and PV demonstrate the differential assault that NMDAR antagonism can have on GABAergic function. When considering the role that these interneurons play in healthy brains, dysregulation of mesolimbic dopaminergic neurons can be linked to what is observed in SZ (Coyle 2012). fMRI studies have also found disrupted connectivity between frontal and temporal regions, relevant when considering these mesocortical and mesolimbic systems (Lawrie et al. 2002).

NMDAR antagonism is hypothesized to result from the neurochemical abnormalities observed in the SZ. Postmortem studies found reduced levels of glutamate and diminished breakdown of the endogenous antagonist, N-acetylaspartyl glutamate (NAAG) in the prefrontal cortex and hippocampus of SZ brains (Tsai et al. 1995) while MRS studies found diminished levels of glutamate and glutamine (glx) in the frontal regions of the brain as well as decreased levels of N-acetyl aspartate (NAA) (Marsman et al. 2011).

Prior to the shift of focus onto NMDAR's role in SZ pathology, aberrations in dopaminergic signaling was the leading hypothesis of SZ pathology due to effects of cocaine and LSD previously mentioned. The hypothesis held hyperactive mesolimbic dopaminergic neurons responsible for the positive symptoms and hypoactive mesocortical dopaminergic neurons responsible for the negative symptoms (Stahl 2007). The effects of current day antipsychotics – both typical and atypical – work best to alleviate positive symptoms due to their affinity for dopamine receptor subtypes (Coyle 2010). They do little towards the relief of negative symptoms, however, suggesting that

dopamine is only half the story. PCP and Ketamine did much to shift the focus onto NMDAR dysfunction within the context of GABAergic and glutamatergic abnormalities. The findings fueled the initial use of the glutamate carboxypeptidase II ($GCPII^{+/-}$) knockout mice as a model of NMDAR antagonism.

$GCPII^{+/-}$ Mouse Model

$GCPII^{+/-}$ mice are heterozygous mutant mice with one of the two copies of the folate hydrolase 1 gene knocked out. It has been hypothesized that this mutation results in diminished levels of the enzyme GCPII (Schaevitz et al. 2011) which is found on astrocytes, supporting cells of neurons, and is responsible for cleaving N-acetylaspartylglutamate (NAAG) to N-acetylaspartate (NAA) and glutamate (Glu) (Fig. 3.).

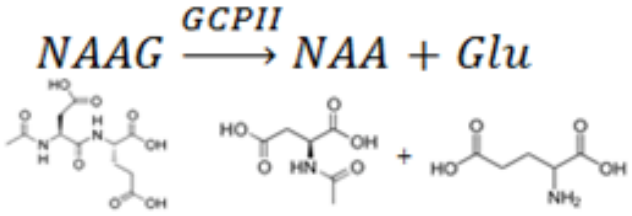

Fig. 3. Enzymatic activity of glutamate carboxypeptidase II cleaving N-acetylaspartylglutamate to N-acetylaspartate and Glutamate.

It was postulated that diminished levels of GCPII would mirror the pathophysiology of SZ by reducing catabolism of NAAG and subsequently reducing levels of glutamate. Lower levels of the agonist glutamate and higher levels of the antagonist NAAG were thought to successfully model NMAR antagonism (Bergeron and Coyle 2012).

Extending the GCPII$^{+/-}$ Mouse Model: Epigenetics

In 1991, Gottesman published findings that demonstrated how the risk of developing SZ increased as a function of the genetic similarity between unaffected and affected (with SZ) relatives. He found that second-degree relatives would have a lesser risk when compared to first-degree relatives, and dizygotic twins would have a lesser risk when compared to monozygotic twins, who exhibited the highest concordance rate of about 50% (Lewis and Levitt 2002). Such findings demonstrated the need to consider the role that both an individual's environment and their genetics play in the predisposition to and development of SZ. A concordance rate below 100% implicates the interactions that take place between genes and the environment (Os et al. 2008). Epigenetics, the heritable or adaptive changes in gene expression comprise these interactions. Such changes in gene expression occur via DNA methylation, and/or modifications in the structure and function of chromatin or histone proteins (Akbarian 2010). Exploration into epigenetic mechanisms was fueled (Akbarian 2010) by the lack of a single genetic abnormality as the cause for the development of SZ (Kaminsky et al. 2009).

Predominant findings among schizophrenics are the diminished expression of the glycoprotein Reelin and glutamic acid decarboxylase-67 (GAD_{67}) (Guidotti et al. 2000). GAD67 is an important GABA synthesis enzyme that utilizes glutamate as a precursor (Guidotti et al 2000). It was posited that such findings were the result of dysregulated epigenetic mechanisms. DNA Hypermethylation of promoter regions as well as increased conversion to repressive chromatin (Huang and Akbarian 2007) have been correlated with these deficiencies. However, this study found that diminished gene expression correlated more with repressive chromatin modifications than with DNA

hypermethylation (Huang and Akbarian 2007). Numerous investigators have proposed that specific modifications to residues on histones are the means of defining active and repressive chromatin (Jenuwein and Allis 2001, Berger 2002, Iizuka and Smith 2003, Peterson and Leniel 2004, Wang et al. 2004).

Schavetiz et al. explored the role of epigenetic regulation by focusing on one carbon metabolism (C1) (Schaevitz et al. 2011). The C1 cycle has been considered the umbrella mechanism under assault in SZ because it plays a role in a number of characteristic abnormalities of the disorder such as aberrant DNA methylation, NMDAR dysfunction and abnormal prenatal levels of folate and homocysteine (Krebs et al. 2009). C1 metabolism consists of three components; the folate cycle, methionine cycle and transsulfuration pathway each of which involve synthesis of nucleotides for maintenance of DNA, transfer of methyl groups deriving from dietary folate and homeostasis of cellular reduction-oxidation reactions respectively (Schaevitz et al. 2011). The methionine cycle mediates DNA methylation and ultimately gene expression and is therefore implicated in epigenetic dysregulation (Krebs et al. 2009). Previously mentioned abnormalities in GAD67 expression have been connected to aberrant hypermethylation of histone proteins which are contingent on the activity of the methionine cycle. Studies of postmortem SZ brain tissues have found both significant hypo and hyper methylation at different genes related to mitochondrial function, and GABAergic and glutamatergic neurotransmission. Diminished levels of folate and hyperhomocysteinemia are predominant findings in SZ (Krebs et al. 2009). Lower dietary intake of folate is proposed to lead to diminished methylation of homocysteine into methionine which can be the cause of elevated levels of homocysteine.

Schaevitz et al. modeled altered C1 metabolism in GCPII+/-mice by subjecting them to a folate deficient diet but found that the mutation and dietary modulation essentially cancelled each other out (Schaevitz et al. 2011). Homocysteine and glycine levels can increase as a result of a folate deficit (Krebs et al. 2009) and the two can subsequently function as NMDAR agonists diminishing the effects of reduced GCPII levels. Wild type mice, however, did exhibit social, motor and cognitive abnormalities when fed a folate deficient diet (Schaevitz et al. 2011). The "reciprocal interaction" between this folate deficient diet and the GCPII knockout suggested the consideration of different ways to induce epigenetic dysregulation in $GCPII^{+/-}$ mice as a way to better model the disorder. Collaboration with the Akbarian lab has led to plans to introduce the complementary DNA (cDNA) of the histone deacetylase enzyme, HDAC1, via the introduction of an adenovirus vector for overexpression in the mouse cortex. HDAC1 has been shown to be significantly elevated in patients with SZ, and these elevated levels were correlated with decreased expression of GAD67 (Sharma et al. 2008). Altering the methylation status in the DNA of $GCPII^{+/-}$ mice was not considered because both hypo- and hyper- methylation have been exhibited in schizophrenics as a function of gene locus and therefore would not be an accurate model of the epigenomic alterations that take place in this disorder (Akbarian 2010). When histone proteins are acetylated, the DNA can be transcribed and the chromatin is open. When the acetyl groups are removed, i.e. the histone is deacetylated, the chromatin is repressed and condensed, transcription is silenced and heterochromatin may form leading to a deficit in gene expression (Akbarian 2010).

It is anticipated that introduction of HDAC1 cDNA will elevate levels of the enzyme and successfully repress a number of genes in the mouse cortex. MRI and

a behavioral paradigm will continue to be used to assess volumetric aberrations in brain structure and social abnormalities. DTI will be implemented in order to explore the effect of genetic and epigenetic assaults on white matter tracts,supplementing the application of MRS which measured levels of choline (cho), creatine (Cr), taurine (Tau), N-acetylaspartate + N-acetylaspartylglutamate (NAA + NAAG) and glutamate + glutamine (Glx).

Role of Metabolites

The metabolites in this thesis were analyzed because of their relevance to neuronal function, neurotransmission, neurodegenerative disorders and the pathology of SZ.

Choline: Levels of the metabolite choline (Cho) can be indicative of the breakdown of myelin or alteration in neuronal membrane compositions (Bracken et al. 2011). In SZ, diminished Cho levels have been observed in the left hippocampus (Maier et al. 1995). Choline levels have been shown to be positively correlated with memory and attention (Bluztajn, 1998). The NMR-visible choline peak is representative of a number of choline-containing compounds such as glycerophosphocholine, phosphatidylcholine and phosphocholine (Govindaraju et al. 2000). Cho serves as precursor to the mononucleotide cytidine diphosphate choline, necessary for phospholipid synthesis, explaining its relevance to membrane structure.

Creatine: The metabolite creatine (Cr) is utilized as an internal standard in a number of MRS studies (Ongur et al. 2009). All reported levels of metabolites in this thesis are ratio values relative to the level of Cr. This metabolite serves to maintain ATP/ADP levels in muscles (Andres 2008) and altogether plays a role in brain metabolism and energy. Although the use of creatine as an internal standard has been questioned, previous

findings in this project have affirmed its use (Mu 2011).

Taurine: Like choline, taurine (Tau) has been shown to be relevant in the maintenance of neuronal cell membranes. It is an amino acid that serves to protect membranes and promote both neuronal growth and survival (Schuller-Levis and Park 2003). SZ patients have exhibited increased levels of Tau in the prefrontal cortex, hypothesized to be in response to metabolic deficiencies (Shirayama et al. 2009). Prior data obtained on GCPII+/- mice mirrored these findings with significantly higher levels of Tau found in the hippocampal region of GCPII+/- mice (Mu 2011).

N-acetylaspartate and N-acetylaspartylglutamate: The metabolites N-acetylaspartate (NAA) and N-acetylaspartyl-glutamate (NAAG) are significant metabolites in SZ research. NAA is a highly relevant metabolite in the nervous system and can indicate the amount of healthy neurons especially since it has been shown to be reduced in brains that have suffered strokes or tumors (Steen et al. 2005). The viability of neurons can be ascertained by the number of spines or synapses, and their size or density (Bracken et al. 2011). A meta-analysis of MRS studies on SZ found that there is a significant reduction of NAA levels observed in the hippocampus as well as cortical gray and white matter in SZ brains (Steen et al. 2005). Significant correlations have also been found with social abnormalities in SZ and NAA metabolite levels (Sigmundsson et al. 2003). NAAG on the other hand is a predominant peptide transmitter released during neuronal depolarization of glutamatergic and GABAergic neurons (Bergeron and Coyle 2012). It is hypothesized to act as an agonist at a subtype of metabotropic glutamate receptors (mGluR3) blocking glutamate release, and an antagonist of NMDA receptors blocking neuronal excitation. When the breakdown of NAAG is slowed down, excitotoxic effects are hindered (Slusher

et al 1999). GCPII, the cleaving enzyme found on astrocytes, has also been shown to regulate the synaptic concentration of NAAG (Tiffany et al. 2001), thus grounding the hypothesis that a reduction of GCPII can result in excess NAAG and therefore NMDAR antagonism.

Glutamate and Glutamine: The final metabolites of interest are glutamate (Glu) and glutamine (Gln). Glutamate is the major excitatory neurotransmitter in the CNS. Following its release into synaptic clefts, it is taken up by astrocytes and converted to glutamine which is then transported to the axon terminals of presynaptic neurons for glutamate synthesis (Marsman et al. 2011). Interest in glutamatergic neurotransmission stemmed from the antagonistic effects of phencyclidine (PCP) and Ketamine on the glutamatergic NMDA receptor (Paz et al. 2008). An increased glutamine/glutamate ratio was reported in rat prefrontal cortex treated with PCP further connecting NMDAR dysfunction with glutamatergic neurotransmission (Iltis et al. 2009).

A review of MRS studies on medial prefrontal cortex and anterior cingulate cortex metabolites in schizophrenic brains found that glutamate levels were reduced and that levels of glutamine were increased (Marsman et al. 2011). Thus a hypoglutamatergic hypothesis of schizophrenia prevailed, which suggested that reduced levels of glutamate and consequent diminished excitation of NMDA receptors cause the major phenotypes of SZ. Yet numerous findings have since shifted the focus onto hyperglutamatergic activity as responsible for the major phenotypes of the disorder (Paz et al. 2008).

Increased levels of glutamate in rodent prefrontal cortex were reported in rats treated with Ketamine (Moghaddam et al. 1997) and were also shown to correlate with social abnormalities induced by PCP (Adams and Moghaddam 1998). Furthermore, PCP-

induced social abnormalities diminished when glutamate release was inhibited, demonstrating the contingency of the relationship between glutamate and analogous phenotypes of SZ (Moghaddam and Adams 1998). Studies in awake animals showed that NMDAR antagonism resulted in increased glutamate neurotransmission mediated by other glutamatergic receptors such as AMPA receptors (Lorrain et al. 2003). fMRI studies in humans also demonstrated increased activity in the prefrontal cortex following exposure to NMDAR antagonists (Breier et al. 1997). Elevated levels of glutamate can produce excitotoxicity which leads to increased neuronal death and apoptosis (Bogaert 2010). They can also disrupt connections between cortical and limbic layers resulting in compromised regulation of different circuits (Paz et al. 2008) Thus, analysis of glutamate levels may help gauge the effect of the GCPII mutation and offer insight on the viability of this mouse model.

Magnetic Resonance (Kolodny Personal Communications 2013, Hashemi 2004)

MRI, DTI and MRS utilize the behavior of nuclei subjected to a magnetic field to render images, diffusion properties and spectra of proton-containing molecules such as water and metabolites, respectively. This thesis exploits the activity of hydrogen protons because of their relevance to biological systems and their relative abundance in both water and fat (Huang 2012). Hydrogen protons are within the subset of nuclear magnetic resonance (NMR) active nuclei because they have an odd number of protons: one. Nuclei are NMR active by virtue of unpaired protons or neutrons leading them to have non-zero spin quantum numbers (I). Nuclei with nonzero quantum numbers have a property called spin which produces a magnetic dipole moment . The nuclear spin

quantum number determines the number of different energy levels nuclei can attain in the presence a magnetic field, in accordance with the following relationship.

$$\#\ \text{Energy Levels} = 2(I) + 1$$

Hydrogen nuclei have a spin quantum number of ½ and thereby two energy levels. The lower energy state occurs when magnetic moment aligns with external static magnetic field (B_0) and higher energy state when the magnetic moment opposes B_0. The net magnetization vector of the magnetic moments aligns with the external magnetic field because the lower energy state is more favorable. According to the classical model of magnetic resonance, as the magnetic moment aligns with or against the external magnetic field, it begins to precess about the external field in response to its force, much like a spinning top in response to gravity (Larmor Precession). The velocity or rate at which it precesses is the Larmor or resonance frequency of the nucleus. This resonance frequency (ω_0) is determined by the strength of the magnetic field (B_0) and the inherent gyromagnetic ratio (γ) of the nucleus, in accordance with the following relationship.

$$\omega_0 = \gamma B_0$$

The resonance frequency of hydrogen nuclei in a magnetic field strength of 9.4 Tesla is 400 MHz.

Radiofrequency coils are composed of loops of wires that function to both transmit an excitation pulse to a sample and receive the signal induced by changes in the magnetic properties of nuclei. The static magnetic field, B_0, and initial net magnetization lie along the upright z axis (Fig. 4.).

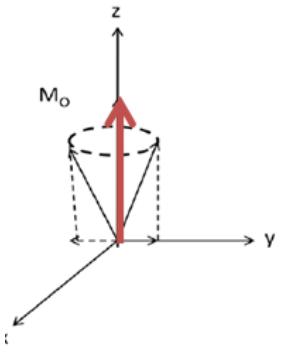

Fig. 4. Net magnetization of magnetic moments align with the static magnetic field along the principal Z axis (Hashemi 2004).

When the magnetic moments are subjected solely to the static B_0 of 9.4 Tesla, their net magnetization lies along the z axis because they are out phase with one another, causing the x and y components of each magnetic moment to cancel. Magnetic moments can be said to project onto the x, y or z axes. In this initial condition, no signal can be obtained because the magnetic moments are neither projecting on the x nor on the y axis. Signal can only be detected within the plane the RF coil receiver lies in, which is the x-y plane. Only the projections of the magnetic moment in this plane can induce current within the coil and thereby manifest as a signal.

In order for these magnetic moments to project into the x and y directions, they must be subjected to a second, weaker magnetic field, B_1, perpendicular to B_0. A radiofrequency (RF) coil delivers an RF pulse tuned to the resonance frequency of the nuclei, producing B_1 and causing the alignments of the magnetic moments to rotate from the z axis to alignment with the x-y plane. The extent of movement the magnetization towards the x-y plane is described by the flip angle, determined by the gyromagnetic ratio and RF pulse duration and strength. Transverse magnetization (in the x-y plane) results when nuclei absorb RF energy at their resonance frequency (Fig. 5.).

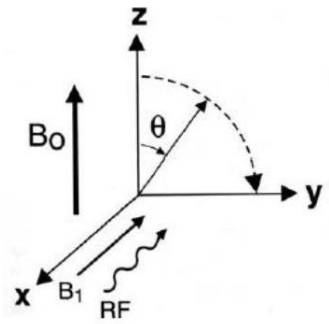

Fig. 5. Magnetic moments absorb energy from RF pulse excitation and move to the transverse plane (Hashemi 2004).

Once in the x-y or transverse plane, nuclei precess about the z-axis in the x-y plane with their characteristic Larmor frequency.

After transverse magnetization is achieved, the RF pulse is turned off leaving the magnetic moments solely subject to the static magnetic field, B_0. The moments begin to dephase in the x-y plane and relax back towards their initial net magnetization with B_0 in a time-dependent manner. T2 is the time constant that describes the dephasing of the magnetic moments, otherwise referred to as transverse relaxation, specifically the time when 63% of the phase coherence is lost. Magnetic moments are also sensitive to magnetic field inhomogeneities and the interaction with other nuclei. This is incorporated into the T2* decay time constant but neglected in T2. The final time constant, T1, describes the relaxation of moments towards the z axis, otherwise referred to as longitudinal recovery, specifically when 63% of the initial net magnetization is recovered.

As the magnetic moments dephase and relax, their projection onto the x-y plane diminishes leading to a decrease in the detected signal. Changes in the x and y components of the magnetic moments induce current in the RF coil producing the

detected signal. The decay of the signal is referred to as the free induction decay or FID. In order to obtain spectrum for MRS or MRI, this FID is fourier transformed.

Magnetic Resonance Spectroscopy (MRS)

MRS is used in this study to probe levels of relevant metabolites. Hydrogen nuclei or protons in different molecules are exposed to magnetic fields distorted due to the electrons surrounding them. These distortions can either enhance or oppose the effect of the static magnetic field, $B_{0,}$ and are dependent on the electron density surrounding the proton (σ). Ultimately, this culminates in an effective magnetic field, B_{eff}, for the nucleus which is determined by the following relationship.

$$Beff = B_0 (1- \sigma)$$

Nuclei, in our case protons, absorb different amounts of energy according to their effective magnetic fields. When the electron density surrounding the nucleus opposes B_0, the nucleus is shielded from the external force. Alternatively, if the electron density of the nucleus aligns with the magnetic field, it is deshielded. Each proton in each type of molecule has a corresponding peak on a spectrum located along the x-axis signifying its chemical shift with parts per million as the unit (Fig. 6.).

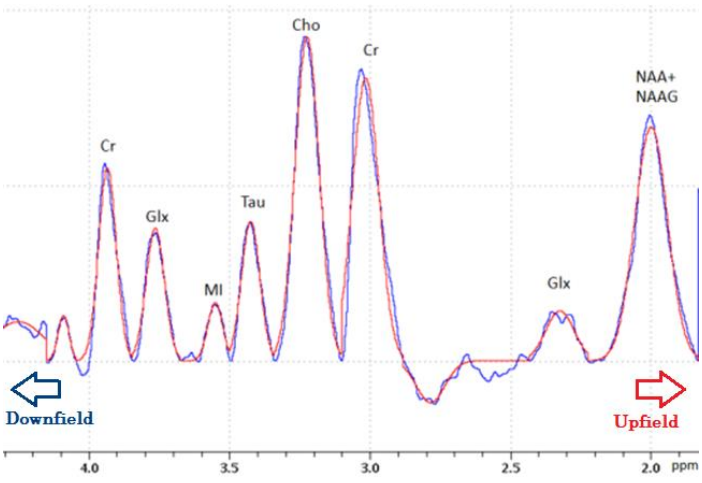

Fig. 6. Proton NMR (1H-MR) spectrum including labeled peaks representative of metabolites with different chemical shifts (Huang 2012)

These peaks are found upfield if the hydrogen nucleus is shielded or downfield if it is deshielded. The amount or concentration of a specific molecule is proportional to the area under the peak. Within any experiment, the chemical shifts of molecules must be compared to a reference frequency. Here the NAA+NAAG peak is used because it is both easily identifiable and clearly resolved in the mouse brain.

It is imperative to have the least field inhomogeneity when obtaining a spectrum. Shim coils throughout the magnet are adjusted, either manually or automatically to homogenize the magnetic field. FASTMAP pulse sequence is used to adjust first and second order shims.

Pulse Sequences

A pulse sequence refers to both the order and components of an imaging or spectroscopy protocol. In general, pulse sequences include components which prepare the sample by suppressing certain signals from water, fat or outer volume, excite the sample and read out the signal. They detail the amount of times the sample is excited (repetitions), the amount of time between each exciting pulse (repetition time; TR), and the amount of time

between the excitation and the readout of the signal or echo, (echo time; TE). When obtaining an NMR spectrum, the Point Resolved Spectroscopy (PRESS) pulse sequence, which consists of three RF excitation pulses in the x, y and z axes with flip angles 90, 180 and 180 respectively, is used along with gradient pulses (Fig. 7.).

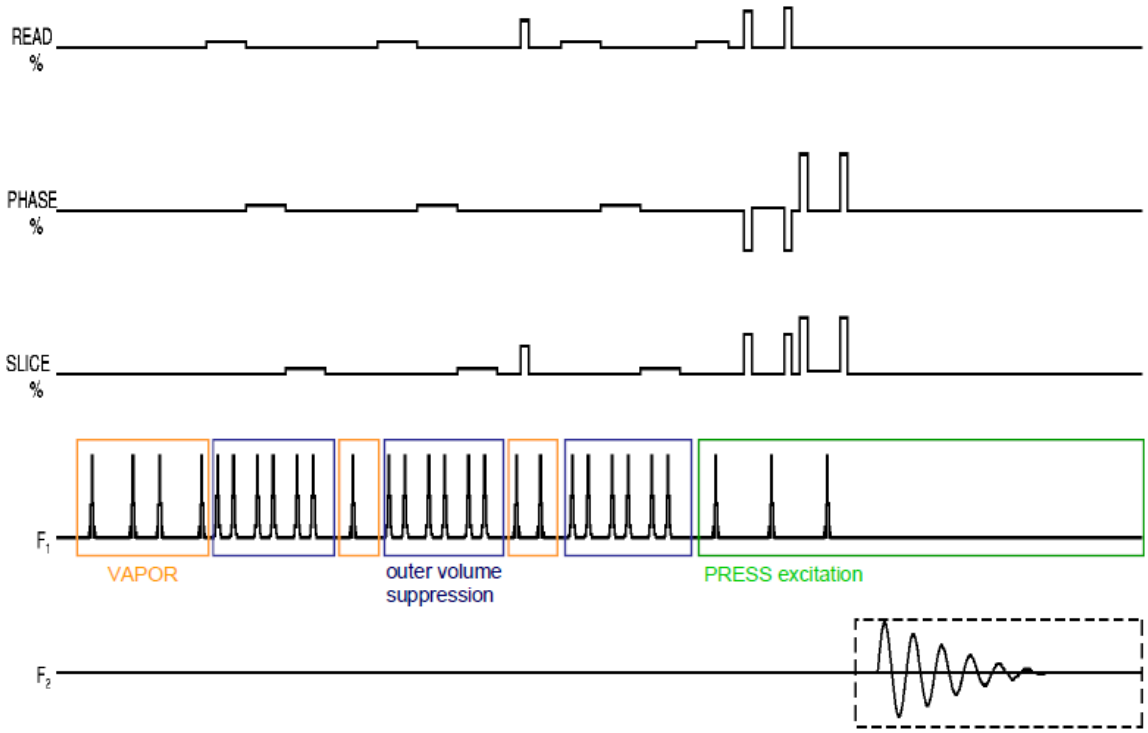

Fig. 7. PRESS pulse sequence demonstrating timing of VAPOR water suppresion, outer volume supression, excitation and signal readout (Bruker Biospin-Measurement Methods 2006).

Gradients function to further distinguish signals by changing the field strength along each principal axis. RF pulses are applied with gradient pulses so that all three (horizontal, coronal and sagittal) planes are sampled. The final signal echo will be the composite of where all of these planes intersect, rendering a single voxel (Yerby 2005). In this thesis, PRESS is used to obtain information from a voxel placed over the hippocampus and cortex. PRESS is coupled with VAPOR water suppression because the signal from water

would overwhelm that from the relatively small concentration of metabolites and outer volume suppression to negate signal from the area outside the voxel (Gujar et al., 2005). Interest in the hippocampus is rooted in its role in learning and memory, an area that patients with SZ have exhibited deficits in. Prevalent findings have also found hippocampal abnormalities in those with SZ (Shenton et al. 2001)

Many of the metabolites of interest are separated from one another along a spectrum because each contains protons subject to different effective magnetic fields, leading to various chemical shifts as the spectrum. Table 2 below includes the chemical structures, predicted chemical shifts and representative experimental spectra for each brain metabolite studied (Govindaraju et al. 2000).

Table. 2. Relevant neurometabolite structures and chemical shifts.

Metabolite	Structure	Predicted Chemical Shift on Proton MRS (ppm)
Cho	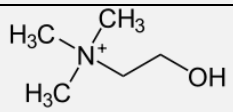	3.1850, 4.0540, 3.5010
Cr	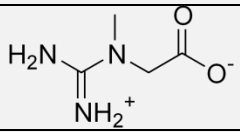	3.0270, 3.9130, 6.6490
Tau	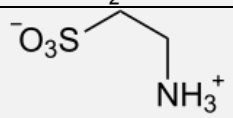	3.4206, 3.2459
NAA	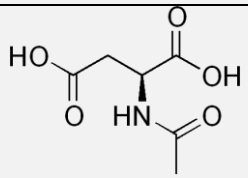	2.0080, 4.3817, 2.6727, 2.4863, 7.8205
NAAG	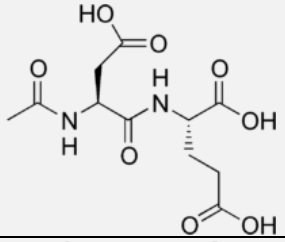	
Glx **Glu**	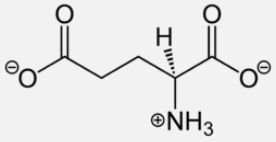	3.7433, 2.0375, 2.1200, 2.3378, 2.3520
Gln	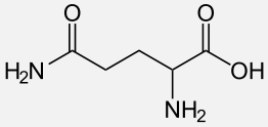	2.1290, 2.1090, 2.3378, 2.4320, 2.4540, 3.7530, 6.8160, 7.5290

Magnetic Resonance Imaging (MRI)

MRI utilizes magnetic field gradients and a spin echo pulse sequence allowing for either T1 or T2 weighted images determined by parameter values for TE and TR (Fig.9.).

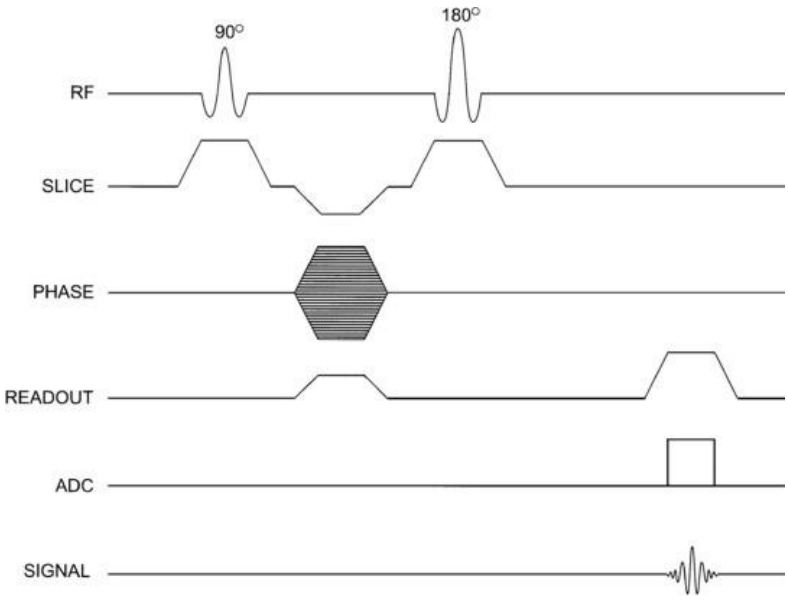

Fig. 8. Spin echo pulse sequence illustrating timing of RF pulse excitation, the slice selection gradient (SLICE) and phase encoding gradient (PHASE) (BITC 2005).

A spin echo pulse sequence includes an initial excitation 90^o RF pulse followed by a 180^o refocusing pulse in order to rephase the magnetic moments which had begun to relax and dephase. This rephasing of the magnetic moments maximizes the subsequent signal (echo) that will be detected by the radiofrequency coil. MRI obtains signal predominantly from water molecules. T1 and T2 weighted images render these tissue-specific signals distinctively. Whereas a T1 weighted image presents fat as bright and water as dark, a T2 weighted image presents water as bright and fat as dark. T2 weighted images are obtained for anatomical data by manually adjusting the TE and TR of the pulse sequence. In order to obtain T2-weighted contrast characteristic of T2 weighted images, both a long TE and a long TR must be adopted. Alternatively, a short TE and short TR would be adopted to

obtain T1-weighted images.

By compartmentalizing the brain into three subtypes of tissue, cerebrospinal fluid (CSF), gray matter and white matter, it is evident how the behavior of water varies according to the tissue type. The more water present in the tissue, the longer it takes for the magnetic moments to dephase in the x-y plane and the slower the longitudinal relaxation. T1 and T2 are properties inherent to the tissue (Fig. 9.).

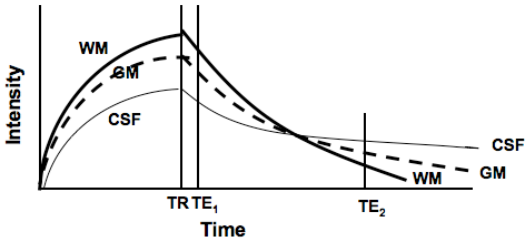

Fig. 9. Longitudinal relaxation (T1) on left and dephasing in x-y plane (T2) on right for gray matter (GM), white matter (WM) ad cerebrospinal fluid (CSF) (Hashemi 2004).

Cerebrospinal fluid thereby has the longest T2 and white matter, being comprised of fat cells, has the shortest. The amount of time following the radiofrequency pulse is crucial in determining which tissue will have greater signal intensity. If the TE is short, signal intensity from fat will be greater than that of water but if it is long, as in our case, water will be bright and fat dark.

Another necessary component in MRI is spatial differentiation. Unlike MRS, it is crucial to determine where specific signal is emanating from in order to visualize a spatial map of the brain. This is achieved by encoding both the frequency and phase of signal within a specific slice. Pulse sequences attain greater complexity when spatial dimensions need to be included by incorporating gradient coils. Frequency, phase and position of magnetic moments are varied and measured with the use of three gradient coils (Gx, Gy, Gz). In this thesis 24 slices are obtained from the caudal to rostral end of the mouse brain, each at

different positions along the z-axis (see below). The slice select gradient G_z alters the static magnetic field along this axis; therefore nuclei at different positions or within different slices resonate at unique Larmor frequencies. The frequency of the RF pulse is fine tuned to this Larmor frequency so that signal is solely obtained from the nuclei within the slice. Signal from the nuclei above or below the slice is effectively silenced. Within the slice, both phase and frequency must be encoded in order to render a spatial map of the sample. The frequency encoding gradient, Gx alters magnetic field strength along the x axis imparting distinct frequencies to magnetic moments. Gy, the phase encoding gradient alters magnetic field strength along the y axis and thereby varies the phase of magnetic moments within a specific position. Each gradient is applied at specific times relative to RF pulse excitations and signal readout (Fig. 10.).

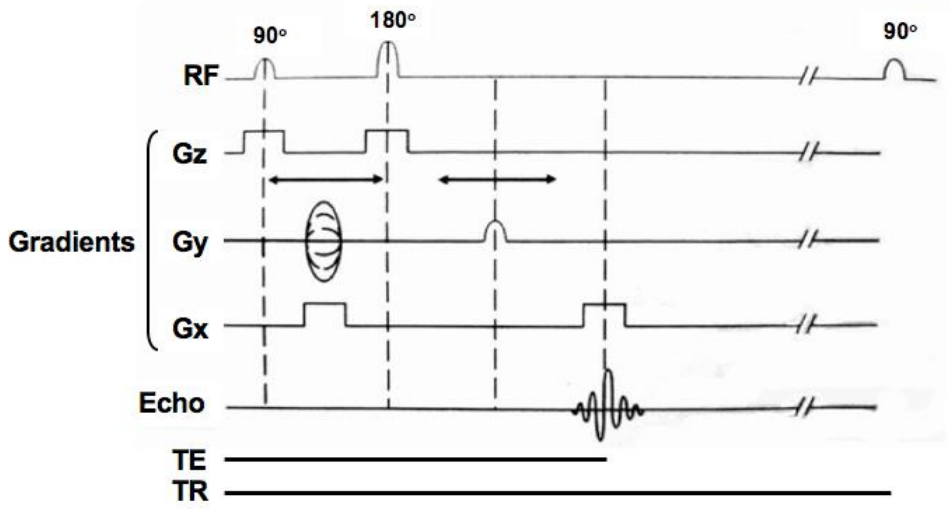

Fig. 10. Application and duration of three gradients in spin echo pulse sequence: slice selection gradient (Gz), phase encoding gradient (Gy) and frequency encoding gradient (Gx) (Hashemi 2004).

The signal encoding phase and frequency is slice specific and stored as an individual data set within k-space, which essentially consists of the raw data from the MRI signal. These raw data must be Fourier transformed in terms of frequency, necessary for the production

of an MR image.

MRI is used to probe brain structures previously implicated in the progression of schizophrenia. Regions of interest include the whole brain, cerebellum, hippocampus and 3rd, 4th and lateral ventricles. A predominant finding in MRI studies on humans with SZ, as mentioned above, has been enlarged ventricles, both third and lateral. Abnormalities have also been exhibited in the hippocampus, frontal and parietal lobes, and cerebellum along with other subcortical and subthalamic structures (Shenton 2010). Enlarged 3rd, 4th and lateral ventricles along with hippocampal asymmetry have previously been found in GCPII$^{+/-}$ mice, consistent with typical findings in those with SZ (Huang 2012).

Diffusion Tensor Imaging (DTI)

Finally, implementation of the diffusion tensor imaging (DTI) protocol will enable the exploration of potential abnormalities in the white matter tracts of the GCPII$^{+/-}$ mouse model. DTI is rooted in the diffusion of water, which can be defined as thermally driven movement throughout the brain also known as Brownian motion (Beaulieu 2002). Different types of tissues subject water molecules to different degrees of obstruction. In cerebrospinal fluid, water is considered isotropic because it is allowed to move in all directions unhindered, but in white matter it is said to be anisotropic because its movement is restricted perpendicular to the axon. (Fig. 11.).

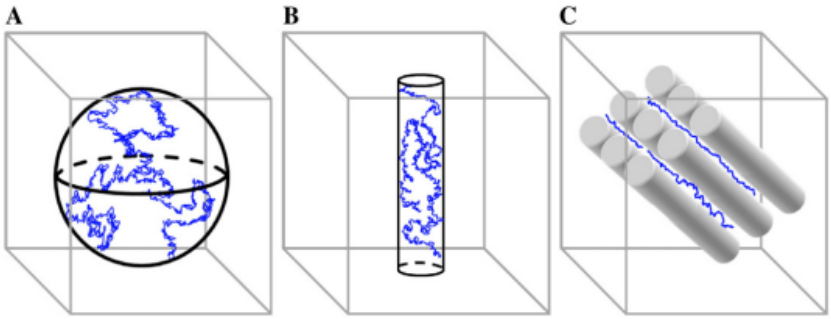

Fig. 11. Water diffusion in isotropic and anisotropic environments. Molecules experience very little obstruction in CSF filled ventricles and can therefore move in any direction (A) in this isotropic environment. Molecules are restricted to move longitudinally within an axon (B) and are highly anisotropic within many axons as in white matter tracts or bundles (C) (Gold et al. 2012).

DTI is the composite of diffusion information acquired from multiple diffusion weighted images (DWI) along several directions (Alexander et al. 2007). A single shot echo planar image (EPI) spin echo pulse sequence is used to acquire each DWI (Fig. 12.).

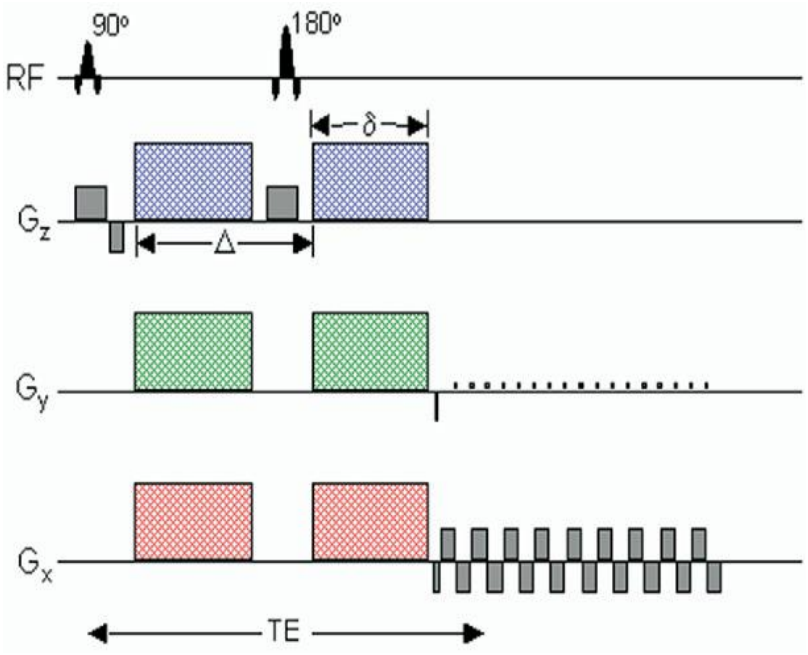

Fig. 12. Single shot EPI based pulse sequence for Diffusion Weighted Image. Gradients (Gx, Gy, Gz) are applied prior to and following the refocusing 180° RF pulse. Multiple echoes are obtained from the signal (Alexander et al. 2007).

This pulse sequence demonstrates how diffusion information is obtained. Through the combination and variation of three gradients along the principal axes, water diffusion can be tracked along different directions. The diffusion coefficient represents the diffusion along the determined direction by the gradient (Maas 2003). The gradients are applied prior to and following the refocusing RF pulse and function to first dephase and then rephase the magnetic moments (Alexander et al. 2007). In stationary tissue, the resulting signal will not be attenuated because the second gradient pulse will ideally undo the effects of the first on the magnetic moments. However, because water molecules move during the time gap between the two gradient pulses, they experience a different gradient strength. This leads to incomplete rephasing and ultimate loss of signal. The diffusion coefficient (D) can be calculated from the loss of signal intensity using the following relationship (Maas 2003).

$$I = I_0^{(-b/D)}$$

The b factor included in the relationship represents the strength, shape and duration of the gradient pulses that are applied (Maas 2003). A given b value is set (786.73 sec/mm^2) that determines the extent of dephasing induced in the sample. I_0 is the measured signal when the b value is 0, when there is no application of gradients, while I is the observed signal once the gradients are applied. A baseline image (b=0) is necessary for any DTI dataset. DWI data are obtained along thirty gradient directions. Diffusion coefficients calculated from these directional samplings comprise the diffusion tensor (LeBihan et al. 2001). The diffusion tensor itself consists of diffusion values along the principal axes of the MR magnet (x,y,z) and the diagonal principal axes of diffusion (xy, xz, yz). This

tensor can be visualized as a 3x3 matrix or as an ellipsoid (Fig. 13.)

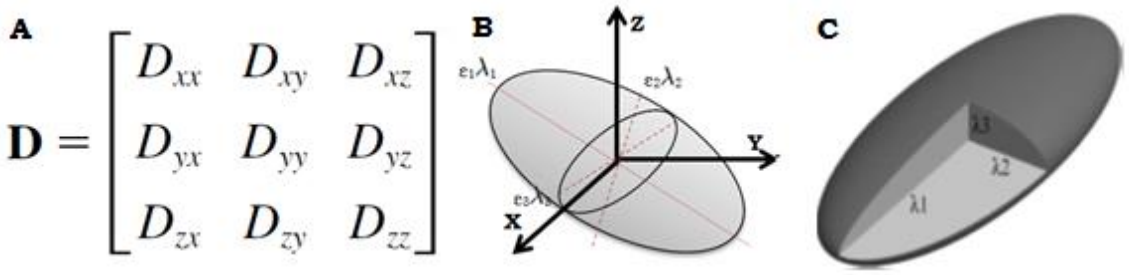

Fig. 13. Representation of the Diffusion Tensor. 3x3 Matrix (A), ellipsoid (B, C). Eigenvalues and eigenvectors adhere to ellipsodial radii along major (1) and minor (2,3) axes. (Thomalla et al. 2004).

The tensor can be used to determine the direction of diffusion along (eigenvectors, ε_1 ε_2 ε_3) and value of diffusivity (eigenvalues, λ_1 λ_2 λ_3) for a given three dimensional tract of the sample. Eigenvalues can be used to determine the fractional anisotropy (FA) of a given white matter tract. FA expresses the extent that water diffusion is restricted by cell cytostructure. Healthy white matter possess a high degree of organization and integrity leading to high FA values while damaged white matter sustaining diminished axonal density and homogeneity produces lower FA values. FA of CSF is standardized at a value of 0. The diagonal elements of the tensor, Dxx Dyy and Dzz, can be used to determine the mean diffusivity (MD) of the sample. MD is equal to the average of the diffusion along the principal axes of the instrument and therefore represents the overall diffusion of water independent of direction. MD values are shown to be indirectly proportional to FA. Greater MD in white matter can signify demyelination or breakdown of neural architecture (Ciccarelli et al. 2003). DTI experiments are being planned to assess the MD and FA of white matter tracts and bundles shown to be damaged in the GCPII$^{+/-}$ mouse model for SZ including cingulum bundle, corpus callosum, internal capsule, fornix, arcuate fasciculus and superior occipito frontal fasciculi (Kubicki et al. 2005). A majority of these connections are concentrated between the frontal and temporal lobes as well as

within the limbic system, regions which have been formerly implicated in the pathology of the disorder.

The goal of this thesis is to further investigate the GCPII$^{+/-}$ mice as a model for the NMDAR dysfunction endophenotype of schizophrenia and ultimately to determine the viability of the model through assessment with MRI, MRS and a behavioral paradigm. Furthermore, this thesis includes the laying of the groundwork for an updated GCPII+/- mouse model and the implementation of DTI as a tool to expand the examination of structural abnormalities. Incorporation of epigenetic dysregulation is motivated in the hope of better mirroring the progression of SZ and exploring the influence of gene expression, and DTI allows for probing of white matter structures which are significantly implicated in the disorder.

Materials and Methods

Animal Model

GCPII+/- mice served as a model for the NMDAR dysfunction endophenotype of schizophrenia in the initial experimental design of this thesis. These mice are heterozygous knockout mice for the folate hydrolase 1 gene responsible for the production of the enzyme glutamatecarboxypeptidase II. GCPII+/- (HET) mice were tested alongside control wild type (WT) C57B1/6J mice. The original GCPII+/- colony was founded at McLean Hospital (Coyle, Belmont, MA). All mice were bred and housed in the Wellesley College Animal Facility where they were subject to a 12 hour light/12 hour dark cycle and a temperature of 21 ± 1°C. Food and water was available *ad libitum*. At postnatal day (PND) 21 mice were weaned and divided into cages according to litter and gender. Ear clipping was used as method of identification for imaging and behavioral experiments. Mouse Genotype (Carlsbad, CA) was responsible for genotyping portion of the study.

Behavioral testing was conducted between PND 114 and 117 in a chambered social apparatus. MRI and MRS portions of the study were conducted on PND 35/36, 49/50 and 63/64 using a 9.4 T Bruker Avance DRX 400 MHz vertical bore NMR spectrometer with a MicroMouse 2.5 imaging accessory (Bruker Biospin, Billerica, MA). Bruker ParaVision 4.0 and Bruker Topspin 1.5 software (Ettlingen, Germany) on a Linux system were used to design and implement scan protocols, obtain data and analyze spectra. MRI and DTI data were analyzed using Analyze 10.0 image analysis software on a Lenovo PC and ParaVision 4.0 ROI tool, respectively. Diffusion Tensor Imaging (DTI) protocol was established with preliminary scans on non-tested C57B1/6J mice.

Behavioral Testing

The social test apparatus, modeled on a prior study on social withdrawal of autistic mice (Moy et al., 2004), was constructed with Plexiglas (Wellesley College Machinist, Estuardo Rodas). The apparatus contains three chambers each 20 cm wide, 22 cm high and 40.5 cm long. The lateral chambers were blocked off from central chambers by dividing walls, but can be made accessible by the removal of sliding Plexiglas doors (Fig. 14.).

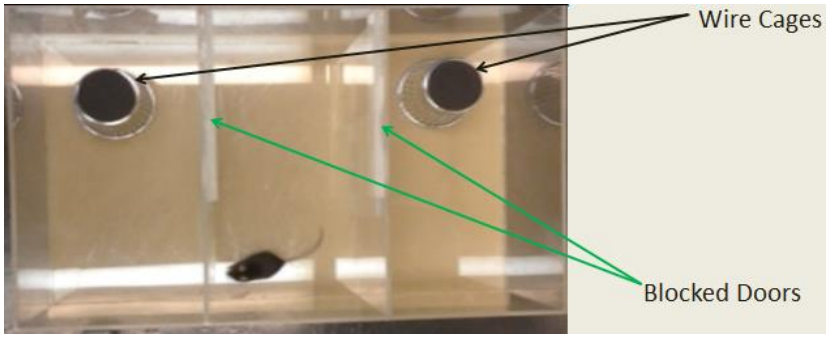

Fig. 14. Camera view of social test apparatus during habituation phase. Wire cages and blocked doors are labeled.

Overturned 4x4x4.25 inch (width x depth x height) steel cages were placed in each of the side chambers (Galaxy Cup, Spectrum Diversified Designs, Inc., Streetsboro OH). Behavioral testing consists of 2 phases: habituation and sociability. During the habituation phase, the test mouse was introduced into the central chamber with the lateral chambers blocked off, and allowed to explore for ten minutes. After ten minutes, the test mouse was removed from the apparatus and placed in a temporary cage on the opposite side of the testing room while the sliding doors were removed and the stranger mouse (Wild Type (WT) male breeder) was confined beneath the steel cage in one of the side

chambers. The test mouse was then reintroduced to the center chamber, commencing the sociability phase. The test mouse's exploratory behavior was videotaped for 10 minutes with a Sony DCR-SX85 digital video camera recorder atop a tripod located 5 feet above and 0.5 feet away from apparatus. All trials were digitally stored and then transferred onto computer for analysis.

Pre-Imaging Procedure

Test mice were anesthetized in a Plexiglas chamber (Braintree Scientific, Inc., Braintree, MA) with 2% Isoflurane in oxygen flowing at a rate of 0.2 L/minute. Mice were subjected to anesthesia for a period of approximately ten minutes until sleep was induced within the chamber, confirmed by the absence of a reflex to a foot pinch. They were then transferred to the Bruker Avance Mouse micro-imaging probe. Mice were secured in the probe with 3M Micropore^{TM} medical tape within a mouse bed equipped with a bite bar (Fig. 15.).

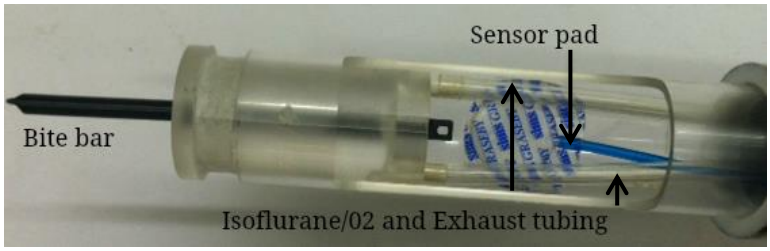

Fig. 15. Aerial view of mouse bed. Labeled sensor pad, bite bar and tubing responsible for inflow and outflow of isoflurane/O_2 gas mixture.

Exposure to anesthesia was sustained when the mouse was in the probe by means of tubing connected to mouse bed. An exhaust tube was connected to both the chamber and the probe in order to contain the contaminated oxygen, and transfer it to a F/AIR Scavenger activated charcoal filter (Paragonmed, Coral Springs, FL). Temperature of the magnet was raised to 32 °C throughout the duration of the experiment to prevent severe

drops in mouse body temperature. Respiratory rate was monitored during imaging session by a respiration sensor pad located beneath the mouse's abdomen on the mouse bed. Sensor pad signals were received by Bruker BioTrig Triggering and Monitory acquisition and command modules, and subsequently visualized onto a C840 Latitude laptop computer with Bruker Biotrig software. Isoflurane levels were modulated using a VIP Veterinary Vaporizer (Colonial Medical Supply Co., Franconia, NH) in order to maintain a respiratory rate within the bounds of 50 to 100 breaths per minute.

Magnetic Resonance Imaging

The imaging probe was first tuned to the resonance frequency of the hydrogen protons at 400 MHz and matched to 50 Ω impedance in order to obtain the highest signal to noise ratio for both the imaging and spectroscopy components of the study. A SINGLEPULSE_1H scan (TR=2665.65 ms, reps=200, averages=1) was used to manually shim and homogenize the magnetic field. To confirm the proper positioning of the test mouse a RARE_tripilot pulse sequence was run (TE=12.5 ms, TR= 2000.000 ms, rare factor=8, matrix size= 128 x 128, averages=1) rendering 3 slices of the mouse brain; sagittal, coronal and horizontal. The entirety of the mouse brain from the cerebellum through the frontal lobe must be within the bounds of the radiofrequency coil in order for a complete set of anatomical images. Anatomical images were obtained using a RARE_8_bas T2 weighted pulse sequence (TE=15 ms, TR= 3109 ms, Tx0 ~15 dB, Tx1~5.2 dB, FOV=2.56 cm^2, averages=16) rendering 24 0.7mm thick coronal slices from cerebellum through frontal lobe (Fig. 16.).

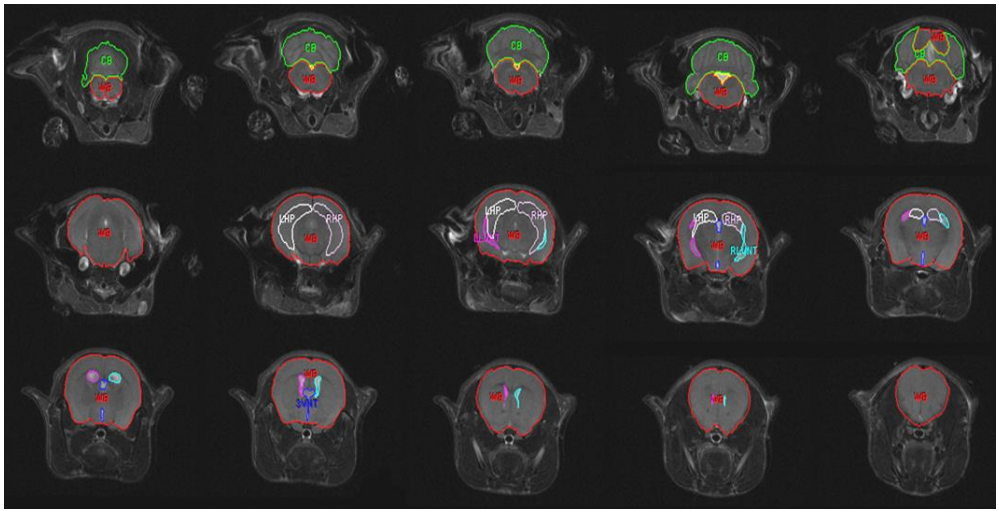

Fig. 16. Representative sample of coronal slices obtained with RARE_8_base pulse sequence. Only 15 slices are shown; tracing of internal and whole structures was accomplished using Analyze 10.0 post data collection.

Magnetic Resonance Spectroscopy

Metabolite levels of the neurotransmitters and neurochemicals creatine, glutamate+glutamine, N-acetylaspartate/N-acetylaspartylglutamate, taurine and choline were determined from a spectrum of the medial region of the hippocampus. A more encompassing region was first delineated with a 4x4x4 mm^3 cuboid voxel of the internal structures on a RARE_8_bas coronal slice (Fig. 17a.). The magnetic field was shimmed over this region with a fastmap_4mm scan. Following shimming, the dimensions of the cuboid voxel were diminished to 4x2x3 mm^3 to closely fit the hippocampus (Fig. 17b.).

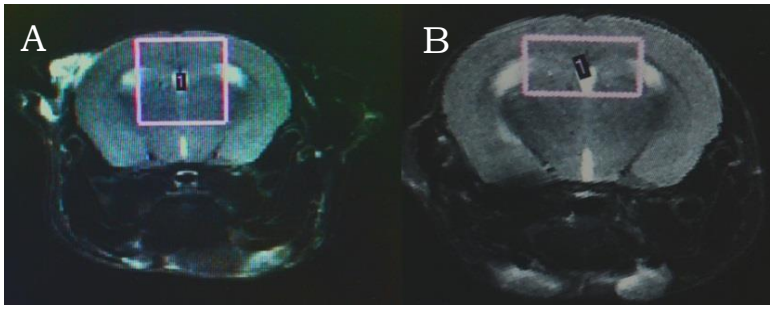

Fig. 17. A. 4x4x4 mm^3 cuboid voxel over hippocampus along with lateral and third ventricles. B. 4x2x3 mm^3 cuboid voxel encompassing medial portion of hippocampus.

Sufficient suppression of the water signal is necessary for greater resolution of metabolite levels. The PRESS_waterline pulse sequence (TE=20 ms, TR= 2000 ms, averages=8) was applied in order to observe a water peak. Bruker TopSpin 1.5 software was used to analyze the obtained water spectrum. A water peak width less than 25 Hz ensured that the homogeneity of the magnetic field was adequate. The PRESS_1H pulse sequence (TE=20 ms, TR=2000 ms, Tx0~150, Tx1~9.4, averages=800) was then used to acquire a spectrum of metabolites. The sequence also reduced signal from water in the tissue and the signal from surrounding tissues.

Diffusion Tensor Imaging

DTI necessitates a modified preparatory fastmap_4mm scan with a 5x5x5 mm^3 voxel to create maximal field homogeneity over internal brain structures. In preliminary experiments designed to learn how to acquire DTI images a RARE_8_bas pulse sequence was used to collect anatomical information. EPI_diffusion_tensor was implemented to obtain diffusion weighted images (TE=33 ms, TR= 2850 ms, matrix size= 128 x 128, slice thickness=0.8 mm, slices= 19, FOV=2.00 cm^2, b= 786.73 s/mm^2, diffusion directions = 30, A0 images=5, averages=10, Tx0 ~7dB, Tx1~0 dB). Nineteen slices of the brain from the cerebellum to the frontal lobe were obtained from this scan. In order to acquire images allowing calculation of the relevant parameters, fractional anisotropy (FA) and mean diffusivity (MD) of different white matter tracts, a post-processing macro was applied, DTI_PROC_TENSOR. This renders 4 different types of images: Fractional Anisotropy, Diffusion Tensor components, eigenvalue images and components of eigenvectors. Paravision 4.0 provides a DTI VISUALIZATION tool to construct color maps from these images and an ROI tool to measure FA and MD.

Data Analysis

Results for male and female mice were analyzed separately.

Behavioral

Digital recordings were observed on either a Lenovo computer or Asus Laptop. Timestamps of the test mouse's entry and exit from each chamber were recorded from the habituation phase over a duration of 10 minutes (600 seconds). The amount of time spent in either the empty chamber or the stranger chamber with the enclosed WT breeder mouse was summed and averaged for each of the four groups of mice: WT males, WT females, HET males, and HET females.

MRI

Anatomical MR images of mouse brain were analyzed using Analyze 10.0 software (Mayo Clinic, Rochester, MN). Whole brain and internal structures: cerebellum, third ventricle, fourth ventricle, left and right lateral ventricles and left and right hippocampus were traced using a Wacom Cintiq 12WX tablet display (Wacom Co., Ltd., Tokyo, Japan). Volumetric measurements were determined by employing the Sample Images tool of the ROI interface which used both the 2-dimensional trace and 0.7 mm slice thickness for volume calculations. Cerebellum and internal structures were traced consistently by one lab member while whole brain was traced consistently by another.

MRS

Bruker TopSpin 1.5 software was used to analyze the metabolite MR spectra. The signal/noise ratio was improved with the application of a linewidth function of 10 Hz. Spectra were then calibrated to the marker N-acetylaspartate/N-acetylaspartylglutamate peak at 2.01 ppm, phased, and fit to baseline. Gaussian fit was used to determine the area

under the peaks and thereby the levels of the metabolite with the creatine peak at 3.0 ppm as an internal standard. The neurometabolities of interest were choline, glutamate/glutamine, N-acetylaspartate/N-acetylaspartylglutamate and taurine.

Statistical Analyses

Statistical tests were conducted separately for males and females.

Social Preference

Student's *t-tests* were used to analyze the amount of time spent in stranger and empty chamber by each genotype group (WT and HET). A paired one-tailed t-test assuming equal variance was conducted for HET mice while a paired two-tailed t-test assuming equal variance was conducted for WT mice. Analyses were conducted in Microsoft Excel and $p < 0.05$ was considered significant.

MRI and MRS

Volume of brain structures and metabolite levels expressed as means were analyzed with repeated measures ANOVAs using genotype as the between group factor with age as the repeated measures. *Post hoc* Tukey's HSD analyses were used to determine the differences between genotype groups as well as between time points. Analyses were conducted in JMP and $p < 0.05$ was considered significant.

Multivariate correlation analysis was also conducted in JMP with pairwise correlation to determine p value for relationship between choline (cho/Cr) and glutamate+glutamine (glx/Cr) levels in female mice.

Results and Discussion

Behavioral Paradigm

Social withdrawal of both wild-type (WT) and GCPII+/- (HET) mice was assessed at a single time point between postnatal day (PND) 114 and 117, approximately 4 months of age. Wild-type mice are expected to exhibit a normal social preference by spending significantly more time in the chamber with the stranger mouse. Alternatively, GCPII+/- or HET mice are expected to exhibit social withdrawal by not spending significantly more time with the stranger mouse. Preliminary behavioral tests conducted on mice ranging from PND 60 to PND 180 demonstrated no social abnormality in HET mice. This was attributed both to testing at premature ages and the wide range in age. In order to offset these confounding variables, a four day time window was designated as the testing period for sociability. Data from male and female mice were analyzed separately in these tests due to the sex differences formerly observed in the $GCPII^{+/-}$ mouse model (Huang 2012).

Both male and female control WT mice (males: n=19; females: n=18) exhibited normal preference by spending significantly more time in the chamber with the stranger mouse (Student's *t*-test: males: $p < 0.05$; females: $p < 0.01$) while both male and female HET mice (males: n=13; females: n=8) showed no preference for the chamber with the stranger mouse (Student's *t*-test: males: $p = .12$; females: $p = .67$) thereby exhibiting social withdrawal (Fig. 18.)

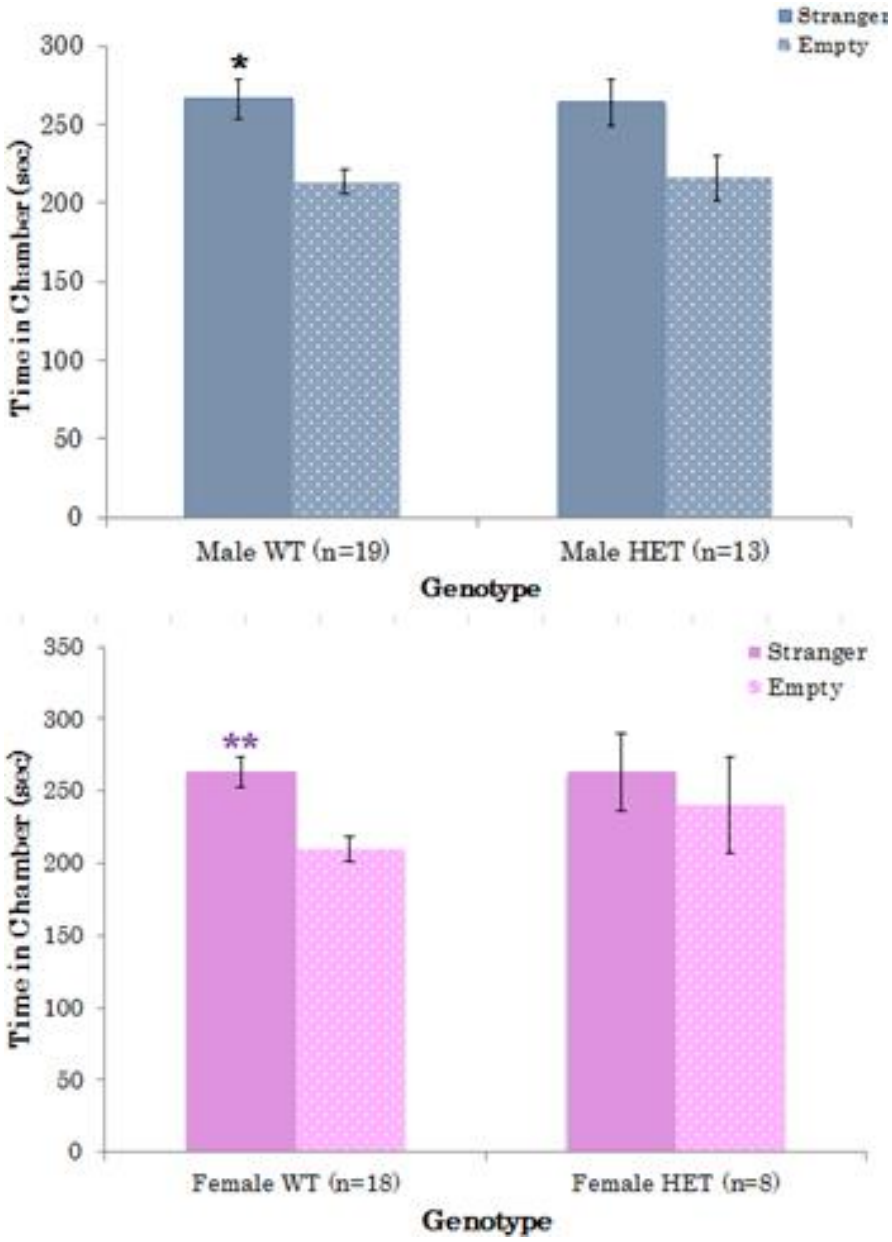

Fig. 18. Male and female GCPII$^{+/-}$ (HET) mice exhibit social withdrawal in comparison to control (WT) male and female mice. Comparing amount of time mouse spent in the empty side chamber (Empty) with that spent in the chamber with stranger mouse (Stranger). Average values shown ± SEM. Sample size (n) included in genotype label. * p <0.05, ** p<0.01.

These findings mirror those from preliminary studies on social interaction in GCPII+/- mice (Han et al. 2009) and support the hypothesis that the GCPII mutation leads to NMDAR dysfunction. Findings agree with those exhibited in mouse models of direct NMDAR antagonism. An earlier study that administered the NMDAR antagonist, MK-

801, to rats found that it induced social withdrawal (Rung et al. 2005). A different study modeled NMDAR dysfunction with genetically modified mice that only expressed 5-10% of the normal levels of a subunit of the NMDA receptor complex, *NR1*, (Mohn et al. 1999) and also found that these mice exhibited social withdrawal. More importantly, this study also demonstrated that clozapine, the leading antipsychotic for schizophrenia, attenuated the social deficit in these mice. Withdrawal from social interaction is a core negative symptom of schizophrenia and this observed social deficit suggest that the GCPII+/- knockout mice can present with phenotypes relevant to schizophrenia, therefore attesting to the model's value.

Magnetic Resonance Spectroscopy and Magnetic Resonance Imaging

Neurometabolite levels of choline, glutamate and Glutamine (Glx), N-acetylaspartate and N-acetylaspartylglutamate (NAA+NAAG) and taurine (Tau) were assessed in both WT and HET mice at three time points following imaging: PND 35/36, PND 49/50 and PND 63/64. Levels were normalized to the internal standard of creatine (Cr). Difficulties in resolving the peaks for N-acetylaspartate and N-acetylaspartylglutamate (NAA+NAAG) resulted in interpretation of the single observed peak as a composite of both metabolites. Such difficulties were also present between glutamate and glutamine (Glx) because of similarities in their chemical shifts. Both an upfield and downfield peak are present in spectra for glutamate. Here the downfield peak is used as the composite of glutamate and glutamine (glx) as glutamate (Fig. 6.).

Volumes of the whole brain (WB), hippocampus (HP/WB), cerebellum (CB/WB), and third (3V/WB), fourth (4V/WB) and lateral ventricles (LV/WB) were measured at same three time points PND35/36, PND 49/50 and PND 63/64 for all mice. Measured volumes

were normalized to the volume of the whole brain. In order to probe structures for asymmetry, the left hippocampi (LH) and right hippocampi (RH) and left lateral ventricles (LLV) and right lateral ventricles (RLV) were measured separately and hippocampal asymmetry (LH/RH) and ventricular asymmetry (LLV/LRV) were determined.

The data were analyzed by gender due to the sex differences previously observed in the $GCPII^{+/-}$ (HET) mice (Huang 2012). Repeated measure ANOVAs were conducted to determine if the factors AGE or GENOTYPE had a significant effect on neurometabolite levels or volume and if there was a significant interaction between AGE and GENOTYPE. Data are presented by factor and interaction within each sex.

Females : Genotype Effect on Metabolite Levels

Analyses found a significant effect of GENOTYPE on levels of glutamate and glutamine (Glx/Cr) [F(1,21) = .575, p <0.01], choline (Cho/Cr) [F(1,21) = .221, p <0.05] and N-acetylaspartate +N-acetylaspartylglutamate (NAA+NAAG/Cr) [F(1,21) = 0.0183, p <0.05] in female mice. GENOTYPE did not have a significant effect on levels of Taurine (Tau/Cr) in females.

Glx/Cr levels were significantly higher in HET females

HET females (n=8) exhibited higher levels of composite Glx than WT females (n=15) did on PND 35/36 (*post hoc*, $p < 0.05$) and PND 49/50 (*post hoc*, $p < 0.01$) (Fig. 19.).

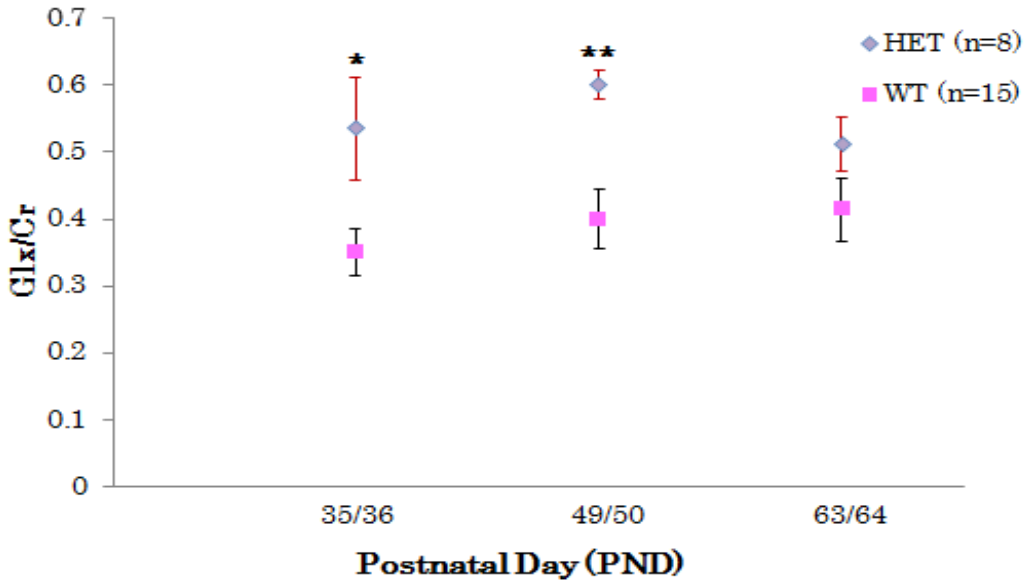

Figure. 19. HET females have higher levels of glutamate and glutamine at PND 35/36 and 49/50. Levels of glutamate normalized to creatine. Repeated measure ANOVAS and Tukey's HSD test *post hoc*. Average values shown ± SEM. Sample size (n) included in genotype label. * p <0.05, ** p<0.01

Higher levels of glutamate may be a function of NMDAR dysfunction mediated by diminished levels of GCPII. Initially the effects of pscyhomimetic drugs like PCP or LSD were interpreted as proof that hypoactive glutamatergic neurons were a fundamental

phenomenon in schizophrenia (SZ) (Paz et al. 2008). Diminished levels and activity of glutamate have been observed in the prefrontal cortex in a number of studies, but recently views concerning the underlying glutamatergic dysfunction have been called into question (Lutkenhoff et al. 2010; Paz et al. 2008).

This recent change in views has been attributed to the failure of NMDAR therapeutic enhancement to alleviate symptoms of SZ (Carpenter and Thaker 2007; Paz et al. 2008) as well as findings of increased glutamate in the striatum and the prefrontal cortex in response to NMDAR antagonism via PCP or other psychomimetic drugs (Bustos et al. 1992; Moghaddam et al. 1997, Paz et al. 2008). Such effects are suggested to result from the role that NMDARs have in the regulation and excitation of GABAergic interneurons. These interneurons, as previously mentioned, function to maintain the balance between excitation and inhibition and their compromised function can manifest in dysregulated activity of glutamatergic neurons, for example.

Cho/Cr levels were significantly higher in HET females

HET females exhibited higher levels of choline (Cho/Cr) than WT females did on PND 49/50 (*post hoc*, $p < 0.05$) (Fig. 20.).

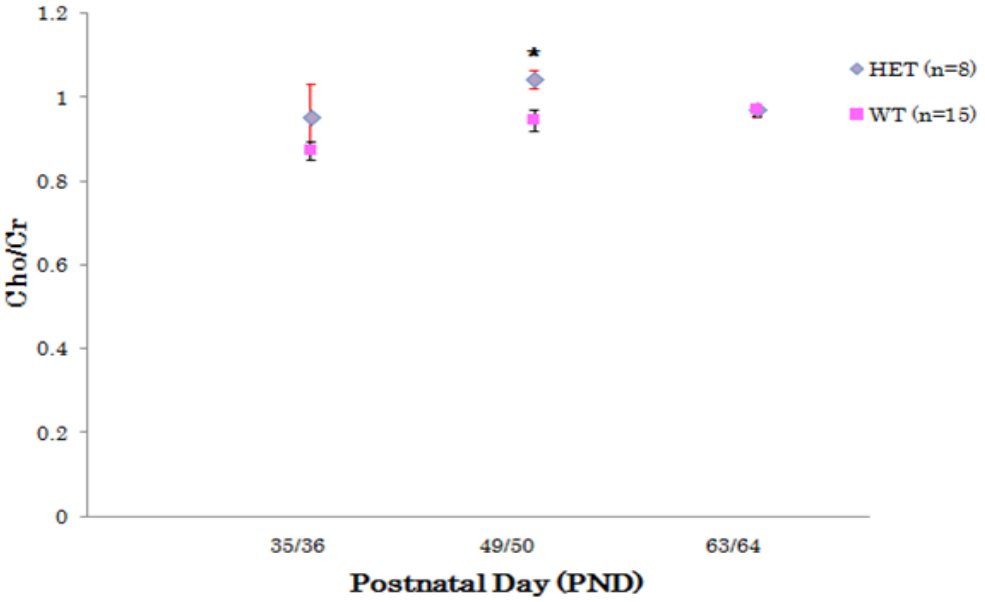

Figure. 20. HET females have higher levels of choline at PND 49/50. Levels were normalized to creatine. Repeated measure ANOVAS and Tukey's HSD *post hoc*. Average values shown ± SEM. Sample size (n) included in genotype. * p <0.05.

Studies on choline levels in patients with SZ are not entirely conclusive. Some studies on the hippocampus of SZ patients observed decreased levels of choline (Maier et al. 1995; Maier et al. 1996, Fukuzako et al. 1995), while others detected greater levels of Cho when comparing patients with their unaffected twins and controls (Lutkenhoff et al. 2010). Choline levels were also found to correlate positively with duration of untreated psychosis (Lutkenhoff et al. 2010). Choline is present in membrane phospholipids, and their increase can signify demyelination or breakdown of neuronal membranes (Théberge et al. 2003). Breakdown of membranes free lipids which are then NMR visible . (Milkevitch et al. 2005). Increases in NMR visible glycerophosphocholine, the choline-

containing membrane phospholipid, are attributed to increased phospholipase A2 activity which in turn is activated by glutamate and NMDA receptors (Milkevitch et al. 2004; Kim et al. 1995; Sandhya et al. 1998). For this reason, Théberge and his colleagues postulate that increased levels of choline could be indicative of hyperglutamatergic activity. Hyperglutamatergic activity causes excitoxicity of neurons leading to apoptosis and cell death (Bear 2006). This hypothesis prompted multivariate correlation analysis on female mice (HET and WT). Analysis revealed a significant positive linear correlation between glutamate and choline on PND 49/50 in female mice (pearson product-moment correlation coefficient: 0.6898; $p<0.001$). Although this correlation does not affirm a causal relationship between glutamate and choline, it is significant to note that its presence coincides with significantly elevated levels of glx/cr and cho/cr in female HET mice. Since the correlation is present in both WT and HET females, these data may show that HET females exhibit abnormal levels of metabolites in response to otherwise normal phenomenon.

NAA+NAAG/Cr levels were significantly lower in HET females

HET females had significantly diminished levels of NAA+NAAG/Cr than WT females on PND 49/50 (p <0.05) (Fig. 21.).

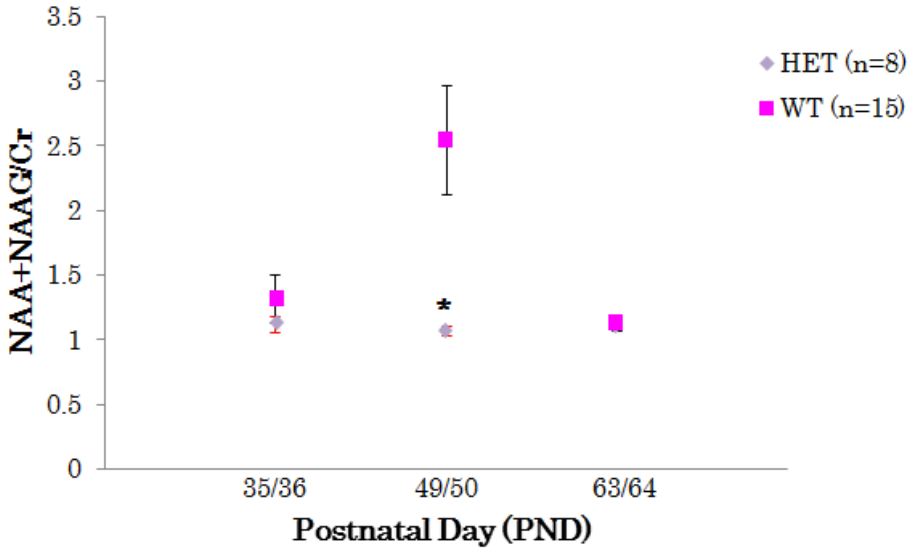

Fig. 21.Female HET mice have lower levels of N-acetyl aspartate and N-acetylaspartylglutamate on PND 49/50. Levels of NAA + NAAG normalized to creatine. Repeated measure ANOVAS and Tukey's HSD *posthoc*. Average values shown ± SEM. Sample size (n) included in genotype. * p <0.05.

The ratio of NAA+NAAG to Glx was calculated and analyzed to further contextualize these differences. GENOTYPE was found to have a significant effect on this ratio [$F(1,20) = .273$, p <0.05].

NAA+NAAG/Glx ratio was significantly lower in HET females

HET females exhibited significantly lower NAA+NAAG/Glx values than WT females did on PND 49/50 (*post hoc*, $p < 0.05$) (Fig. 22.).

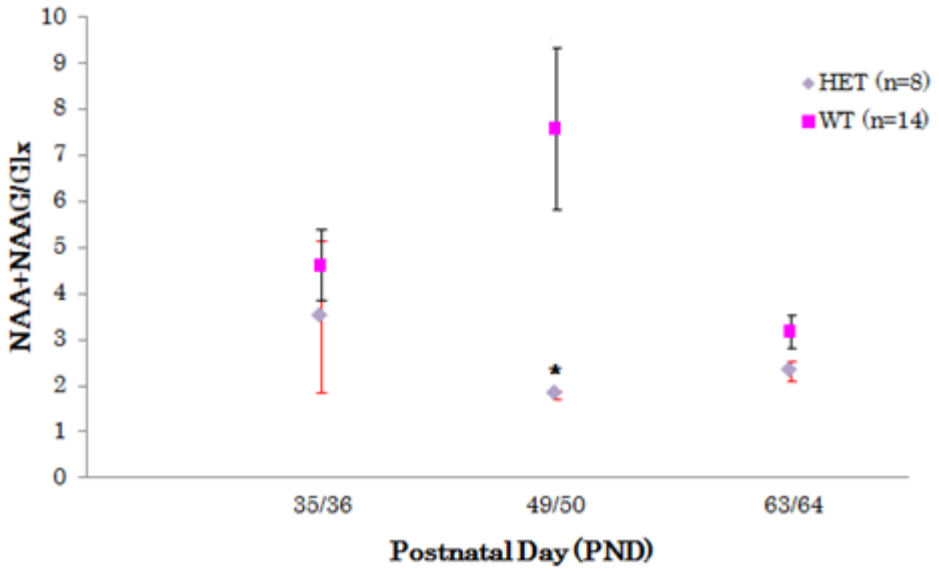

Fig. 22.Female HET mice have lower ratio value of NAA+NAAG/Glx at PND 49/50. Levels of all metabolites were normalized to creatine and measured NAA+NAAG was divided by measured Glx Repeated measure ANOVAS and Tukey's HSD *posthoc*. Average values shown ± SEM. Sample size (n) included in genotype. * p <0.05.

Female mice exhibit a decreased NAA+NAAG/Glx (p<0.05) profile consistent with findings of elevated levels of glutamate and decreased levels of NAA+NAAG in other laboratories. Diminished levels of NAA have been reported in a number of proton MRS studies of the hippocampus in schizophrenics (Harrison 1999; Maier et al. 1995; Bertolino et al. 1996; Deicken et al. 1997, 1998). This phenomenon has been documented in drug-naïve, newly diagnosed and chronic schizophrenic patients (Bertolino 1998) as well as in adolescents, children and unaffected siblings (Bertolino A., Kumra S, Callicot J.H. et al. 1998). Female and male mice are sexually mature by 6-7 weeks therefore the middle time point used in this study can be considered analogous to adolescence in

human beings. NAA reduction has been linked to neuronal loss and dysfunction, tying it to structural abnormalities that have been observed in schizophrenia (Harrison 1999). Reduced levels of NAA also have been tied more specifically to NMDAR dysfunction by the documented effects of the receptor agonist phencyclidine (PCP) (Reynolds et al. 2005). Although Reynolds et al. did not demonstrate reduced NAA levels in the hippocampus, it functioned to show the interaction effect of NAA levels and PCP administration in the striatum and temporal and frontal cortices that correlates with findings in SZ. The GCPII+/- mutation may yield diminished levels of NAA because of the adverse effect it has on NMDAR activity.

Males: Genotype Effect on Metabolites

Analyses found that GENOTYPE did not have a significant effect on neurometabolite levels; Glx/Cr, Cho/Cr, NAA+NAAG/Cr, Tau/Cr or on the NAA+NAAG/Glx ratio values in male mice. However, *post hoc* tests did find significant differences in NAA+NAAG/Glx levels between HET and WT males.

NAA+NAAG/Glx ratio was significantly higher in HET males

HET males exhibited increased ratio of NAA+NAAG/Glx on PND 49/50 (*post hoc*, $p < 0.05$) (Fig. 23.).

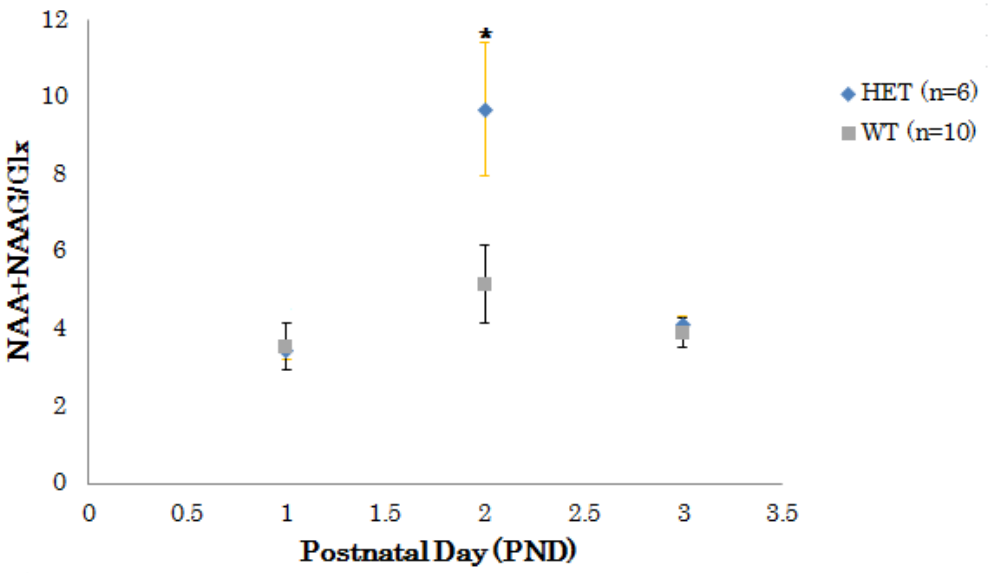

Fig. 23.Male HET mice exhibit higher NAA+NAAG/Glx values at PND49/50 . Levels of all metabolites were normalized to creatine and measured NAA+NAAG was divided by measured Glx. Repeated measure ANOVAS and Tukey's HSD *posthoc*. Average values shown ± SEM. Sample size (n) included in genotype. *$p < 0.05$.

Findings of increased NAA+NAAG/Glx levels in HET males contrast with the reversed trend seen in HET females. Such an aberration can indicate either or both decreased glutamate and glutamine, as well as increased NAA+NAAG. These findings are

inconsistent with the literature which suggests decreased levels of NAA and increased levels of glutamate (Bertolino1998).

The absence of a significant genotype effect on neurometabolite levels juxtaposed the significant genotype effect on social preference seen in both male and female mice. Mice are behaviorally tested at approximately 16 weeks of age while imaging is conducted within 5 and 9 weeks of age. The size of the imaging probe used restricts the period of observation because mice grow too large over time. Thus, the imaging period may be too premature for more NMR-visible changes in male mice to occur.

Females: Genotype effect on brain structures

Analyses found GENOTYPE had a significant effect on hippocampal (HP/WB) volume [F(1,22) = .261, p<0.05] in females. No significant effect was observed on ventricular (3V/WB, 4V/WB, LLV/WB, LRV/WB), cerebellar (CB/WB) or whole brain (WB) volumes.

Hippocampal volume was slightly higher in HET females

HP/WB volume was not significantly different in HET females from WT females at any point but was slightly higher in female HETs at PND 49/50 (*post hoc*, p=0.053) and PND 63/64 (*post hoc*, p =0.053) (Fig. 24.).

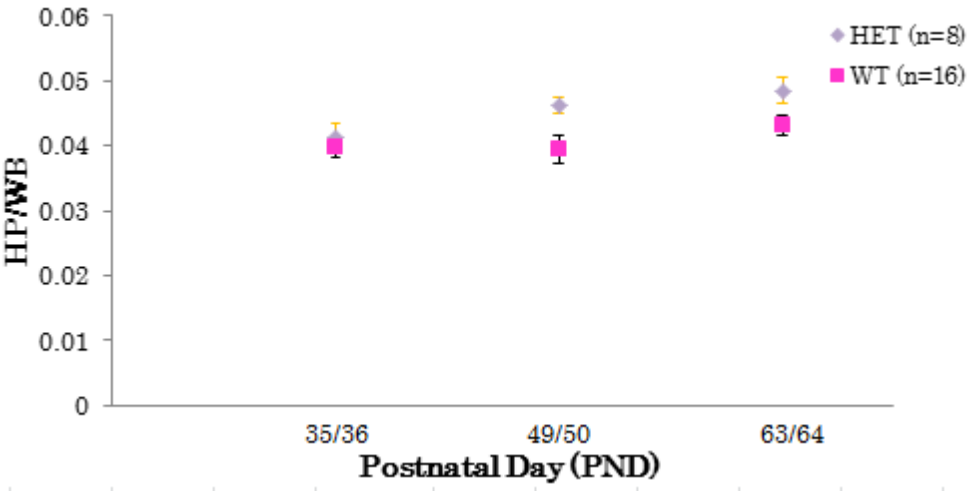

Fig. 24.Female HET mice exhibit slightly higher hippocampal volume at PND49/50 and PND 63/64 and both sets of female mice exhibit increase in hippocampal volume over time. Volumes were normalized to whole brain. Repeated measure ANOVAS and Tukey's HSD *posthoc*. Average values shown ± SEM. Sample size (n) included in genotype.

The hippocampus is implicated in both the symptomology and pathophysiology of SZ. This structure is composed of two main classes of neurons, glutamatergic pyramidal neurons and GABAergic interneurons, making it an extremely relevant arena for adversities of SZ (Heckers and Konradi 2002). Studies have attributed reduced volume of

the hippocampus to loss in the amount of white matter, specifically the GABAergic interneurons (Corter et al. 1987; Benes et al. 1998).Furthermore studies found depleted levels of GABA synthesis enzymes and upregulated GABA receptors in SZ patients. Such findings were attributed to underactivation of NMDAR (Benes et al. 1996, 1997; Heckers et al. 2002). NMDA receptors play the unique role of activating these GABAergic interneurons, and their localized dysfunction in a subset of these GABAergic interneurons has been attributed to aberrant neural activity and morphology (Nakazawa et al. 2012).

Males: Genotype effect on brain structures

Analyses found GENOTYPE had a significant effect on hippocampal asymmetry (ratio of left hippocampus to right hippocampus; LH/RH) [F(1,23)= .519, p<0.01] and on right hippocampal volume (RH/WB) [F(1,23) = .186, p <0.05]. No significant effect was reported for ventricular (3V/WB, 4V/WB, LLV/WB, LRV/WB), cerebellar (CB/WB) or whole brain (WB) volume.

Hippocampal asymmetry was significantly greater in HET males

Male HET mice had significantly greater hippocampal asymmetry compared to WT males at PND 49/50 (*post hoc*, p <0.01) (Fig. 25.)**.**

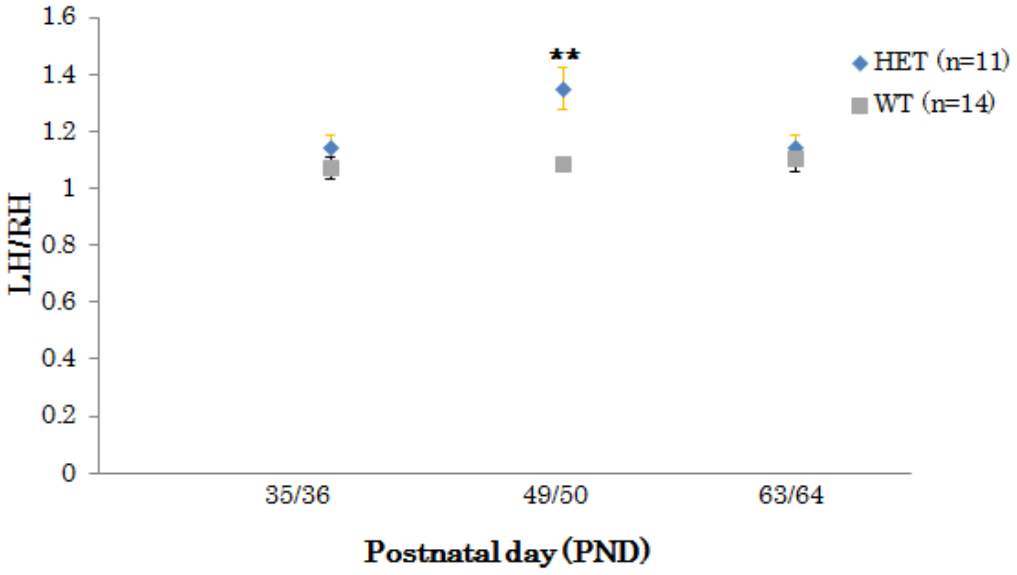

Fig. 25.Male HET mice exhibit higher hippocampal asymmetry at PND 49/50. Volumes were normalized to whole brain. Repeated measure ANOVAS and Tukey's HSD *posthoc*. Average values shown ± SEM. Sample size (n) included in genotype. *p <0.05, **p <0.01.

Right hippocampal volume was significantly lower in HET males

HET males have significantly smaller RH/WB volume than WT males on PND 49/50 (*post hoc*, $p<0.05$) (Fig. 26.)

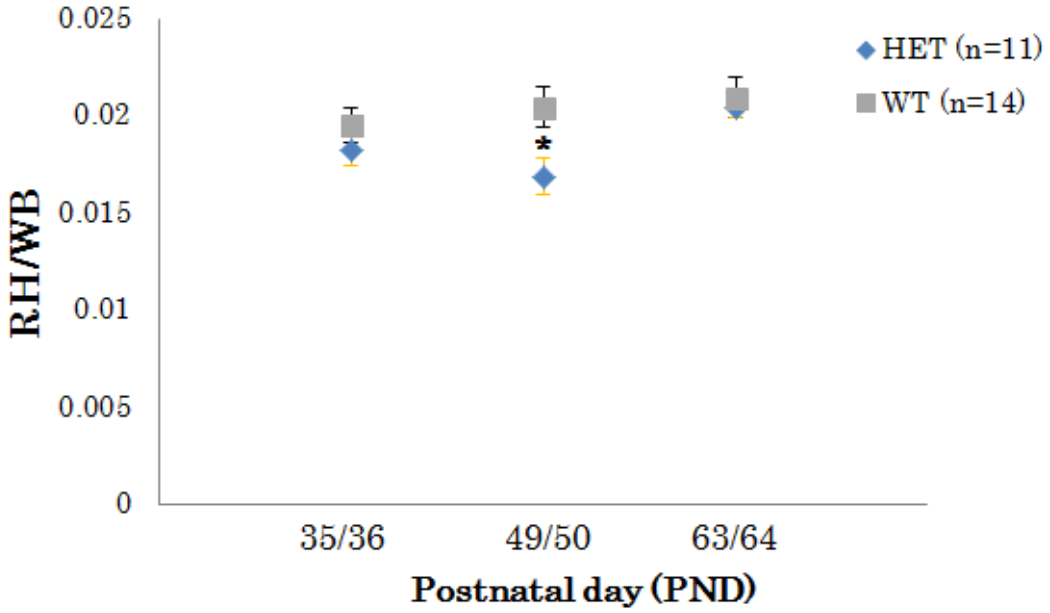

Fig. 26.Male HET mice exhibit smaller right hippocampus at PND 49/50. Volumes were normalized to whole brain. Repeated measure ANOVAS and Tukey's HSD *posthoc*. Average values shown ± SEM. Sample size (n) included in genotype. * $p<0.05$, ** $p<0.01$

In this project neither male nor female mice exhibited a genotype effect on the volume of the third, fourth or lateral ventricles although ventricular enlargement is a major abnormality found in SZ. Shenton and his colleagues report that in about 80% of 55 studies enlarged lateral ventricles were found, with a more exaggerated effect on the left (Shenton et al. 2001). Whereas lateralization of abnormalities is exhibited by both the hippocampus and lateral ventricles in SZ, neither male nor female mice exhibited a GENOTYPE effect on lateral ventricle asymmetry while HET males did exhibit hippocampal asymmetry. Hippocampal volume is found to be diminished in the majority of studies on SZ with more reduction seen in the left side (Shenton et al. 2001; Velakoulis et al. 1999). HP/WB volume deficits have also been recently utilized as

predictors in children at risk for developing SZ.

Female HET mice exhibited increased total hippocampal volume as opposed to findings of reduced hippocampi in the literature. The Male HET mice exhibited a significantly higher hippocampal L/R ratio at PND 49/50 consistent with lateralization of hippocampal reduction seen in SZ although the lateralization in GCPII+/- male mice is in the left as opposed to the right. The mutation is nevertheless correlated with bringing about an endophenotype mirroring what is seen SZ.

The cerebellum is a region of the brain traditionally important for motor control but due to the connections it sustains with limbic structures and cortical areas important for cognitive faculties, its role in cognitive function has been reconsidered. Studies on SZ have not found major abnormalities in the gray matter of the cerebellum but have shown trends of increased white matter (Levitt et al. 1999). Increased white matter has been linked to compromised circuitry intrinsic to the cerebellum, and leading to cognitive dysfunction characteristic of SZ (Schmahmann 1996). As previously mentioned, however, no significant effects or differences were found in cerebellar to whole brain volume in either male or female mice.

Females: Age Effect on brain metabolites

Analyses reported AGE had a significant effect on NAA+NAAG/Glx ratios [F(2,19) = .465, p <0.05] and Tau/Cr levels [F(2,20)=0.508, p < 0.05]. AGE did not have a significant effect on Cho/Cr, Glx/Cr or NAA+NAAG/Cr levels.

NAA+NAAG/Glx ratio values decrease over time in female mice

NAA+NAAG/Glx ratio values were not significantly different between any time points, but were slightly higher on PND 49/50 compared to values on PND 63/64 (*post hoc*, p=0.09) (Fig. 22.).

Tau/Cr levels significantly decreased over time in female mice

Taurine levels were significantly lower on PND 49/50 and PND 63/64 than at PND 35/36 (*post hoc*, p<0.05) (Fig. 27.).

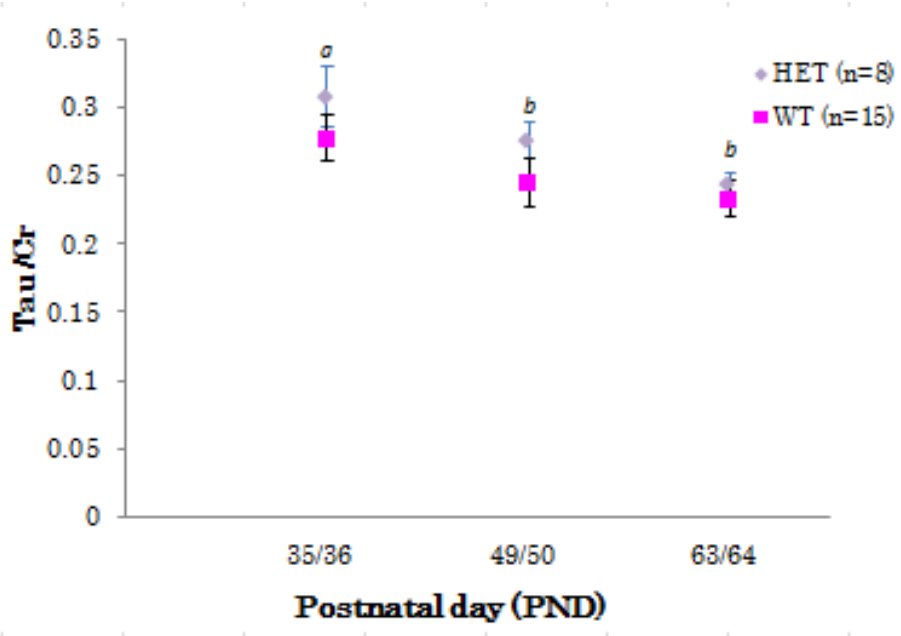

Fig. 27.Female mice exhibit lower levels of Taurine at PND 49/50 and PND 63/64 compared to PND 35/36. Levels of Taurine normalized to creatine. Repeated measure ANOVAS and Tukey's HSD *posthoc*. Average values shown ± SEM. Sample size (n) included in genotype. Letters denote significant differences between time points *a*, b *p<0.01*.

Decrease in taurine levels can suggest diminished maintenance of neurons and neuronal membranes. However, these findings can also be interpreted to reflect a decreased need for neuronal upkeep as the mice fully mature. Studies on those with SZ have found increased levels of taurine and have attributed them to a potential increased need for protection against oxidative stress (Shirayama et al. 2009). Genotype does not have a significant effect in this case and the decrease of taurine over time can be indicative of a normal process.

Males: Age Effect on metabolites

In male mice, AGE was found to have a significant effect on levels of Cho [F(2,13) = 1.264, p <0.01] and NAA+NAAG[F(2,13) = 1.172, p<0.01] as well as on the NAA+NAAG/Glx ratio values [F(2,13) = 1.87, p <0.01].

Cho/Cr levels increased over time in male mice

Cho levels were not significantly different between any time points but were slightly higher on PND 63/64 compared to PND 35/36 (*post hoc*, p = 0.6) (Fig. 28.).

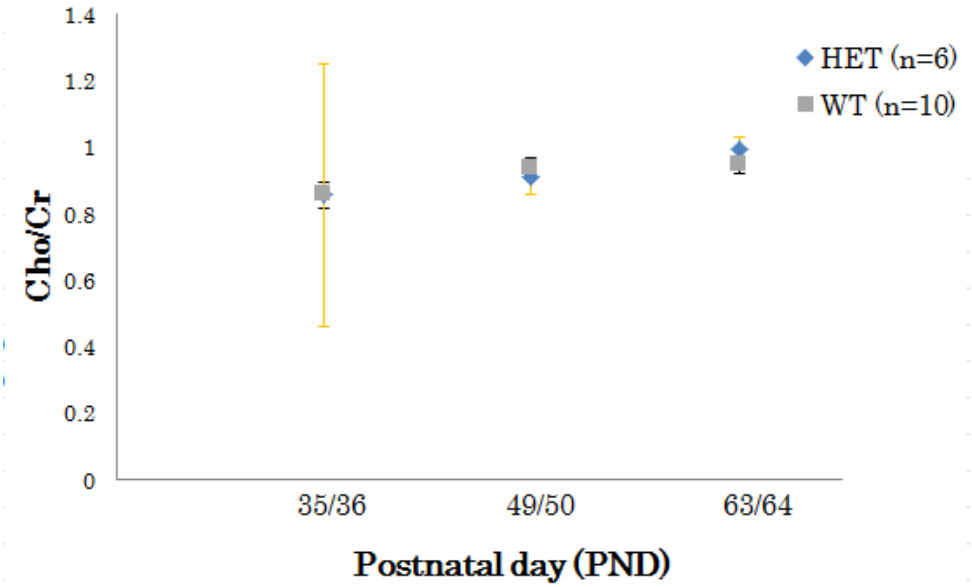

Fig. 28. Male mice exhibit slight increase in Choline levels over time. Levels of Cho normalized to creatine. Repeated measure ANOVAS and Tukey's HSD *posthoc*. Average values shown ± SEM. Sample size (n) included in genotype.

NAA+NAAG/Cr levels peak in male mice

NAA+NAAG/Cr levels were significantly higher on PND 49/50 compared to PND 35/36 (*post hoc*, $p < 0.05$)and PND 63/64 (*post hoc*, $p < 0.01$) (Fig. 29.)

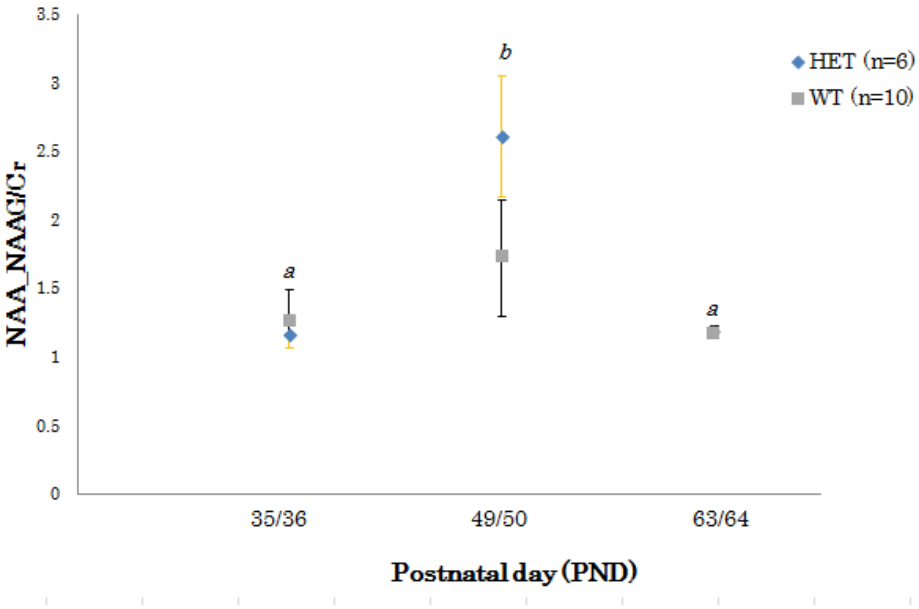

Fig. 29. Male mice exhibit higher levels of N-acetylaspartate and N-acetylaspartylglutamate at PND 49/50 compared to PND 35/36 and PND 63/64. Levels of NAA +NAAG normalized to creatine. Repeated measure ANOVAS and Tukey's HSD *posthoc*. Average values shown ± SEM. Sample size (n) included in genotype. Letters denote significant differences between time points *a*, b *p<0.01*.

NAA+NAAG/Glx ratio values peak in male mice

NAA+NAAG/Glx ratio values were signifiantly higher on PND 49/50 compared to PND 35/36 (*post hoc*,$p < 0.01$) and PND 63/64 (*post hoc*, $p < 0.01$) (Fig. 30.)

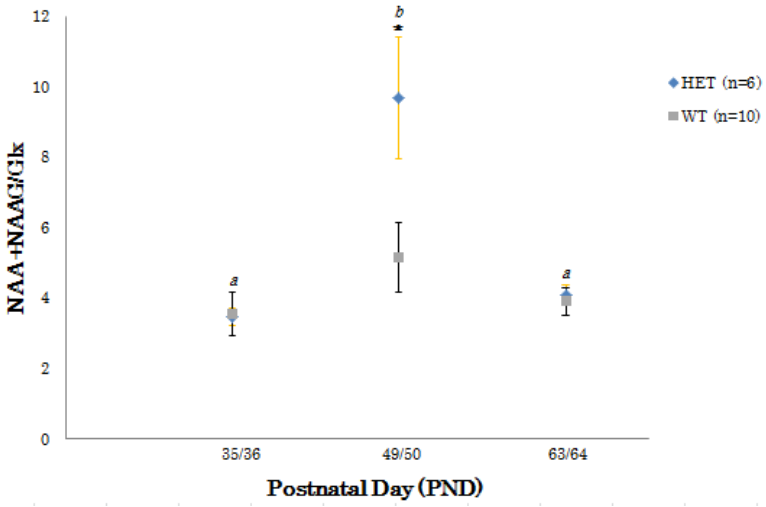

Fig. 30. Male mice exhibit higher levels of N-acetylaspartate and N-acetylaspartylglutamate at PND 49/50 compared to PND 35/36 and PND 63/64. Levels of all metabolites were normalized to creatine and measured NAA+NAAG was divided by measured Glx. Repeated measure ANOVAS and Tukey's HSD *posthoc*. Average values shown ± SEM. Sample size (n) included in genotype. Letters denote significant differences between time points *a*, b $p<0.01$.

Females: Age Effect on brain structures

Analyses found that AGE had a significant effect on hippocampal (HP/WB) [F(2,21)=.44, p<0.05] and lateral ventricle (LAT/WB) volume [F(2,21) = .39, p <0.05]. AGE did not have a significant effect on the volume of other brain structures; cerebellar, whole brain, lateral ventricular asymmetry, 3rd ventricle, 4th ventricle, and hippocampal asymmetry.

Hippocampal volume increased over time in female mice

Although HP/WB volume was not significantly different between time points, it was slightly greater on PND 63/64 compared to PND 35/36 (*post hoc*, p = 0.0635) (Fig. 24.).

Lateral ventricular volume increased over time in female mice

Similar to HP/WB, LAT/WB volume was not significantly differently between time points but exhibited higher HP/WB volume on PND 63/64 compared to PND 35/36 (*post hoc*, p = 0.06) (Fig. 31.).

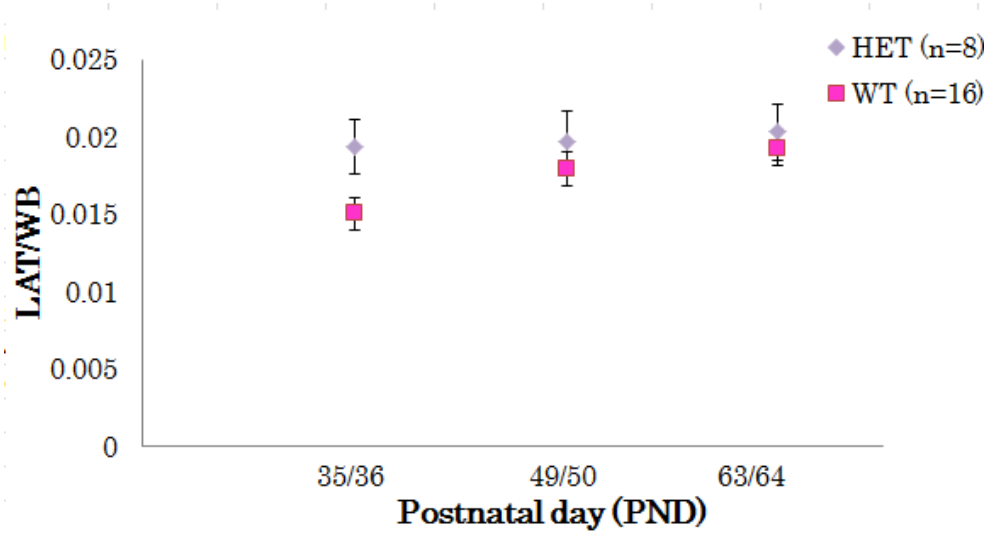

Fig. 31. Female mice exhibit small increase in lateral ventricle volume over time. Volume were normalized to whole brain. Repeated measure ANOVAS and Tukey's HSD *posthoc*. Average values shown ± SEM. Sample size (n) included in genotype.

Male: Age Effect on brain structures

Analyses found that AGE had a significant effect on HP/WB volume [F(2,22) = .320, p <0.05]. AGE did not have a significant effect on the volume of other brain structures; cerebellar, whole brain, lateral ventricular asymmetry, 3rd ventricle, 4th ventricle, lateral ventricle and hippocampal asymmetry.

Hippocampal volume increased over time in male mice

Although HP/WB volume was not significantly different between time points, it was slightly greater on PND 63/64 compared to PND 35/36 (*post hoc*, p = 0.09) (Fig. 32.).

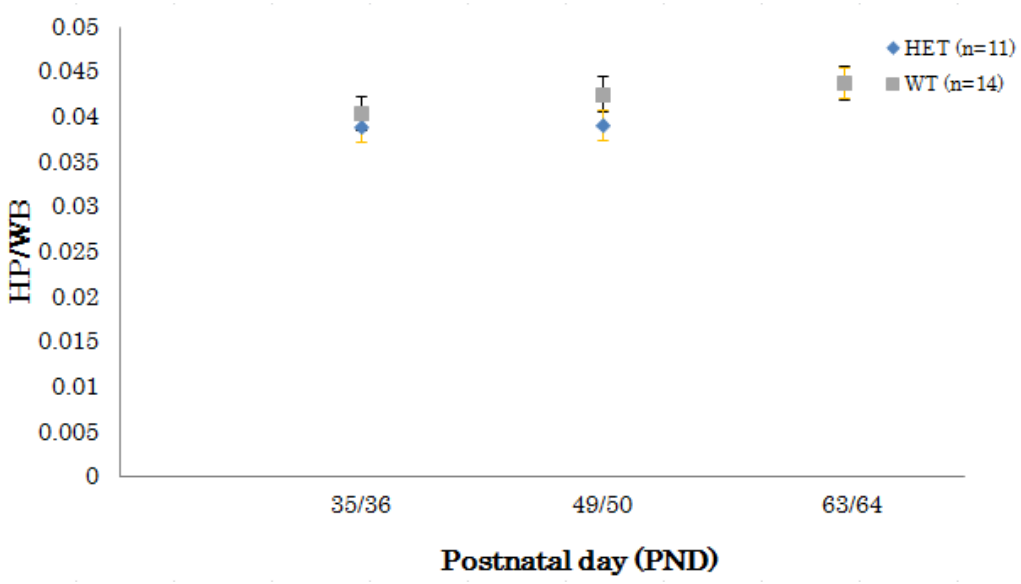

Fig. 32. Male mice exhibit small increase in hippocampal volume over time. Volumes were normalized to whole brain. Repeated measure ANOVAS and Tukey's HSD *posthoc*. Average values shown ± SEM. Sample size (n) included in genotype.

Females: Genotype x Age Interaction

Analyses reported did not find the interaction between GENOTYPE and AGE to have a significant effect on metabolites; Cho/Cr, Glx/Cr, NAA+NAAG/Cr, Tau/Cr or brain structures; CB/WB.

Males: Genotype x Age Interaction

Analyses found that the interaction between AGE and GENOTYPE had a significant effect on NAA+NAAG/Glx ratio values [$F(2,13) = .616$, $p < 0.05$]. The interaction between AGE x GENOTYPE was not significant on any other neurometabolites; Cho/Cr, NAA+NAAG/Cr, Glx/Cr, nor any other brain structure volumes; cerebellar, lateral ventricles, 3rd ventricle, 4th ventricle, whole brain, hippocampus, lateral ventricular asymmetry, hippocampal asymmetry.

NAA+NAAG/Glx ratio peaks

HET males had a significantly higher NAA+NAAG/Glx ratio on PND 49/50 in comparison to PND 35/36 and PND 63/64 in HET males (*post* hoc, $p < 0.01$). WT males exhibited the same trend with the NAA+NAAG/Glx ratio peaking at PND 49/50 relative to PND 35/36 (*post hoc*, $p = 0.3$) and PND 63/64 (*post hoc*, $p = 0.4$) but differences were not significant (Fig. 33.)

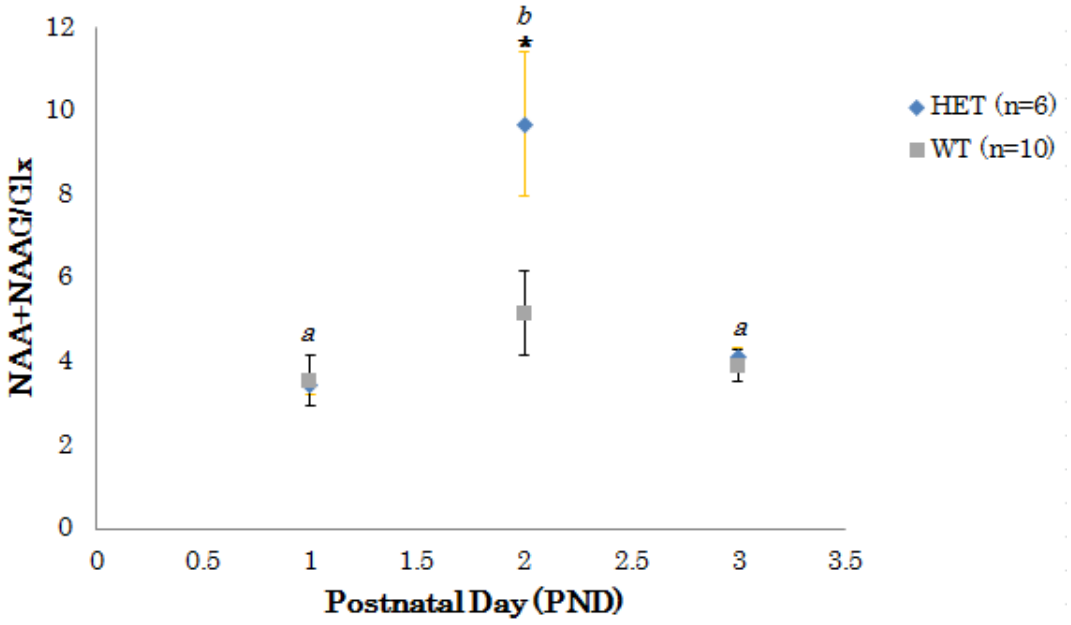

Fig. 33. Male HET exhibit different trend in NAA+NAAG/Glx ratio values over time Levels of all metabolites were normalized to creatine and measured NAA+NAAG was divided by measured Glx.. Repeated measure ANOVAS and Tukey's HSD *posthoc*. Average values shown ± SEM. Sample size (n) included in genotype. Letters denote significant differences between time points *a*, *b* $p<0.01$

While genotype effects offer the best support for the viability of the GCPII mutation in eliciting SZ pathology, consideration of the different trends in structural volumes and metabolite levels between male and female mice can also provide evidence further linking the mutation with NMDAR dysfunction and ultimately SZ.

Sex Differences in SZ (Leung and Chue 2000)

This final discussion section outlines the ways different findings for male vs. female mice are comparable with those in human studies, as well as the potential cause for this difference (see table 3).

Table 3. Composite sex differences in MRI and MRS findings.

Effect	Males	Females
Genotype Effect	Higher NAA+NAAG/Glx at PND 49/50 in HET males Greater hippocampal asymmetry at PND 49/50 in HET males Smaller right hippocampus at PND 49/50 in HET males	Lower NAA+NAAG and NAA+NAAG/Glx at PND 49/50 in HET females Greater hippocampal volume at PND 49/50 and PND 63/64 in HET females Higher Glx at PND 35/36 and 49/50 in HET females Higher Cho at PND 49/50 in HET females
Age Effect	Slight increase in Cho over time Increased NAA+NAAG at PND 49/50 Slight increase in hippocampal volume over time	Slight decrease in NAA+NAAG and Tau levels over time Slight increase in hippocampal and lateral ventricular volume over time
Genotype x Age Interaction	Higher NAA+NAAG/Glx in HET males at PND 49/50	None on neurometabolites None on volumes of brain structures

A review of human studies reveals that males with SZ exhibit more structural abnormalities than schizophrenic females. Similarly, this project found that male HET mice exhibited significantly greater hippocampal asymmetry and lower right hippocampal volume compared to male WT mice. While female HET mice solely exhibited significantly higher total hippocampal volume compared to female WT mice. Lateralization of brain abnormalities, specifically in the hippocampus, is predominant in

males with SZ and is correlated with greater impairments to language processing. Some studies have found that males with SZ perform poorer in learning and memory tasks compared to females with SZ. Here, male HET mice exhibit hippocampal asymmetry and reduced right hippocampus at the same time female HET mice exhibit enlarged total hippocampal volume. Brain asymmetry observed in healthy brains offers insight into differential development of SZ. Healthy female brains have higher gray matter to whole brain values in the hippocampus as well as other cortical and temporal lobe areas, which has been attributed to having a protective role against cell death. Schizophrenic male brains exhibit more reduction in both temporal lobe structures and enlarged lateral ventricles with lateralized reduction in the left hemisphere.

Although male HET mice closely mirror these structural abnormalities, female HET mice sustain the bulk of abnormal neurometabolite levels relevant to the disorder. Studies have contended that SZ male brains exhibit reductions in N-acetylaspartate levels and elevations of choline levels. These neurochemical aberrations are instead observed in female GCPII$^{+/-}$ (HET) mice. While male HET mice better model structural abnormalities relevant to SZ pathology, female HET mice may prove to be a better model for the neurochemical abnormalities characteristic of SZ.

Age of onset is another characteristic of SZ that differs among sexes, with males experiencing onset earlier (ages 18 -25) than females (ages 25-35, 40). This project similarly found that age interacts with genotype differently in males vs. females. Male mice exhibited a significant GENOTYPE x AGE interaction on NAA+NAAG/Glx ratio values, while female mice did not. It is crucial to take the age of mice during testing into account. MRI and MRS are conducted at 5, 7 and 9 weeks of age, all of which correlate

with mouse adolescence during times of sexual maturity and changing hormonal levels. The significance of hormones is evident from findings on females with SZ. Antipsychotics are observed to be more effective in reproductive females and higher doses are needed in post-menopause females. Treated females also improve faster and to a greater extent than treated males. Investigations into these differences have identified the class of hormones, estrogens as the culprit tipping the balance. The estrogen hypothesis of schizophrenia is centered on the fact that estrogens play an important role in neurodevelopment by regulating the organization and structure of circuits throughout maturation and maintain a preventative antipsychotic role. Males exhibit slower development of neuronal connections and prolonged axonal myelination which is attributed to greater testosterone levels as opposed to estrogen.

Estrogens are postulated to bear an antipsychotic role because diminished levels are directly correlated with increased severity and presentation of symptoms. This is characteristic of the period of menopause. It is hypothesized that the increased rate of late age onset of SZ in females is due to decreased levels of estrogens resulting from menopause. Estrogens have been shown to modulate dopaminergic activity by regulating receptor affinity and synthesis, tying it to aberrant dopaminergic activity that is a marker for the disorder. Estrogens also facilitates synaptogenesis, more specifically that of excitatory connections including NMDAR and therefore is also connected to glutamatergic neurotransmission.

Estrogens may be at the root of the sex differences in subject mice and may also explain the concentration of differences in HET females at PND 49/50. Neurometabolite levels are disproportionately aberrant in female HET mice but not in male HETs. This can be

attributed to a potential interaction with the GCPII mutation, NMDAR dysfunction and estrogen levels resulting in compromised protection of neurochemistry. PND 49/50 is right at the cusp of sexual maturity and thus could be the time when estrogen levels have begun to rise (Mayer et al. 2010). Abnormalities may be present at PND 49/50 because estrogens are still increasing and they're could be a latency for their effect. Following this time point, PND 49/50, estrogens are thought to be elevated to be at their highest, which could possibly explain why many of the neurochemical aberrations are normalized by the later time point, PND 63/64.

Conclusions and Future Work

The GCPII$^{+/-}$ mouse model is a promising start to mirroring relevant and characteristic endophenotypes of schizophrenia. This project found that genotype had a significant effect on the volume of brain structures, neurometabolite levels and sociability. Hippocampal asymmetry and lateralized hippocampal reduction in male GCPII$^{+/-}$ HET mice on PND 49/50 resonated with findings in males with SZ. Increased levels of choline coupled with decreased levels of N-acetylaspartate and N-acetylaspartylglutamate in female GCPII$^{+/-}$ HET mice on PND 49/50 accurately reflect neurochemical abnormalities prevalent in SZ studies. Social withdrawal in both male and female HET mice was also observed. However, genotype was not found to play a role in male neurometabolite levels and only a subtle role on female hippocampal volume.

The incorporation of epigenetic dysregulation and diffusion tensor imaging (DTI) propels this project into the current sphere of schizophrenia research. More attention is being given to the interaction between genes and environment as playing a major role in the progression and development of this disorder. Probing of white matter with DTI offers a novel perspective into structural abnormalities that may be considered more relevant for NMDAR dysfunction and SZ pathology as opposed to gray matter. This can be argued because NMDA receptors sustain a role in the formation and maintenance of connections that comprise tracts and bundles of axons throughout the central nervous system. Assessment of the viability of these tracts can indicate if NMDAR are functioning properly.

Future goals of this project will be to solidify the procedure for neonatal rodent surgeries to introduce histone deacetylase enzyme 1 (Hdac1) into the cingulate cortex, and western

blotting and in situ hybridization to confirm overexpression of the enzyme. The extended mouse model incorporates this introduction of histone deacetylase enzyme 1 cDNA (HDAC1) via an adeno-associaed virus (AAV) on the day of birth. Both GCPII+/- and WT mice will undergo this procedure, along with sham injections to control for potential confounding errors, resulting in six experimental groups; HET/AAV, WT/AAV, HET/saline, WT/saline, HET and WT.

The DTI procedure must also be utilized to collect and analyze data along with continued anatomical and behavioral assessments. A final goal for this project could be to incorporate a pre pulse inhibition task as a behavioral assessment due to the translatability of the findings from rodents to humans and the predominance of the deficit in those who suffer from schizophrenia (Powell et al. 2009).

References

Akbarian S. Epigenetics of SZ. Behavioral Neurobiology of SZ and Its Treatment. 2010.611-628.

Alexander A.A., Lee J.E., Lazar M., Field A.S. Diffusion Tensor Imaging of the Brain. Neurotherapeutics. 2007. 4:316-329.

Anaesthesia UK. (2009 Dec 1). NMDA Receptor. Clinical Anasthesia. Retrieved March 25th, 2013 from http://www.frca.co.uk/article.aspx?articleid=100515#.

Andreasen, N.C. SZ: From Mind to Molecule. Washington, DC: American Psychiatric Press, Inc. 2005.
Association, A.P. Diagnostic and statistical manual of mental disorders. 4th ed. 2000. doi:10.1176/appi.books.9780890423349

Bear MF, Connors BW, Paradiso MA Neuroscience: Exploring the Brain.2006.

Beaulieu C. The basis of anisotropic water diffusion in the nervous system- a technical review. NMR Biomed. 2002. 15:435-455.

Bergeron R., Coyle J.T. N-Acetyl Aspartyl-glutamate, NMDA Receptor AND psychosis. Curr Med Chem. 2012. 19(9):1360-1364.

Bertolino A, Kumra S, Callicott JH *et al*. Common pattern of cortical pathology in childhood-onset and adult-onset schizophrenia as identified by proton magnetic resonance spectroscopic imaging. *American Journal of Psychiatry*.1998. 155:1376–1383.

Bertolino A, Nawroz S, Mattay VS, Barnett AS, Duyn JH, Moonen CT, et al. Regionally specific pattern of neurochemical pathology in schizophrenia as assessed by multislice proton magnetic resonance spectroscopic imaging. Am J Psychiatry.1996.153: 1554–1563.

Blanke ML, VanDongen AMJ. Activation Mechanisms of the NMDA Receptor. In: Van Dongen AM, editor. Biology of the NMDA Receptor. Boca Raton (FL): CRC Press; 2009. Chapter 13.

Bogaert, E., d' Ydewalle, C., and Van Den Bosch, L. Amyotrophic Lateral Sclerosis and Excitotoxicity: From Pathological Mechanism to Therapeutic Target, Cns & Neurological Disorders-Drug Targets.2010.9:297–304.

Bracken, B. K., Jensen, J. E., Prescot, A. P., Cohen, B. M., Renshaw, P. F., and Ongur, D.Brain metabolite concentrations across cortical regions in healthy adults, Brain Research.2011.1369: 89–94.

Breier A, Malhotra AK et al. Association of ketamine-induced psychosis with focal activation of the prefrontal cortex in healthy volunteers. Am J Psychiatry. 1997.154: 805–811.

Bustos G, Abarca J, Forray MI, Gysling K, Bradberry CW, Roth RH. Regulation of excitatory amino acid release by N-methyl-D-aspartate receptors in rat striatum: in vivo microdialysis studies. Brain Res. 1992. 585:105–115.

BITC. (2005 May 8). Sequence Diagrams. Biomedical Technology Center. Retrieved March 20th, 2013 from http://bitc.bme.emory.edu/seq_dia.html.

Carpenter WT, Thaker GK. Evidence-based therapeutics--introducing the Cochrane corner. Schizophr Bull. 2007. 33:633–634.

Ciccarellie O., Werring D.J., Barker G.J., Griffin C.M., Wheeler-Kingshott C.A.M., Miller D.H., Thompson A.J. A study of the mechanisms of normal appearing white matter damage in multiple sclerosis using diffusion tensor imaging Evidence of Wallerian degeneration. J Neurol. 2003. 250: 287-292.

Coyle, J.T. NMDA Receptor and Schizophrenia: A Brief History. Schizophrenia Bulletin. 2012. 38 (5): 920-926.

Coyle, J. T., Balu, D., Benneyworth, M., Basu, A., Roseman, A. Beyond the dopamine receptor: novel therapeutic targets for treating SZ. Dialogues in Clinical Neuroscience. 2010. 12(3): 359-382.

Crow T.J. Molecular Pathology of SZ: more than one disease process. British Medical Journal. 1980.66-68.

Deicken RF, Zhou L, Corwin F, Vinogradov S, Weiner MW. Decreased left frontal lobe N-acetylaspartate in schizophrenia. Am J Psychiatry. 1997. 154: 688–690.

Deicken RF, Zhou L, Schuff N, Fein G, Weiner MW. Hippocampal neuronal dysfunction in schizophrenia as measured by proton magnetic resonance spectroscopy. Biol Psychiatry.1998. 43: 483–488.

Fukuzako H, Takeuchi K, Hokazono Y *et al*. Proton magnetic resonance spectroscopy of the left medial temporal and frontal lobes in chronic schizophrenia: preliminary report. Psychiatry Research: Neuroimaging. 1995. 61:193–200.

Galderisi S., Vita A., Rossi A., Stratta P., Leonardi M., Maj M., Invernizzi G. Qualitative MRI findings in patients with schizophrenia: a controlled study. Psychiatry Research: Neuroimaging. 2000. 98:117-126.

Glantz LA, Lewis DA. Decreased dendritic spine density on prefrontal cortical pyramidal neurons in schizophrenia. Arch Gen Psychiatry.2000. 57:65–73.

Gold B.T., Johnson N.F., Powell D.K., Smith C.D. White Matter integrity and vulnerability to Alzheimer's disease: Preliminary findings and future directions. Biochim Biphys Acta. 2011.1822:416-422.

Gottesman, I.L. SZ genesis: The origins of madness. A series of books in psychology. New York,NY: W H Freeman/Times Books/ Henry Holt & co.1991.

Govindaraju, V., Young, K., and Maudsley, A. A. (2000) Proton NMR chemical shifts and coupling constants for brain metabolites, NMR Biomed.2000.13, 129–153.

Guidotti A., Auta J., Davis J.M., Di-Giorgi-Gerevini V., Dwivedi Y., Grayson D.R., Impagnatiello F., Pandey G., Pesold C., Sharma R., Uzunov D., Costa E. Decrease in reelin and glutamic acid decarboxylase67 (GAD67) expression in SZ and bipolar disorder:a postmortem brain study. Arch Gen Psychiatry. 2000.57:1061-1069.

Grunze HC, Rainnie DG, Hasselmo ME, Barkai E, Hearn EF, McCarley RW, Greene RW. NMDA dependent modulation of CA1 local circuit inhibition. J Neurosci.1996.16:2034–2043

Han, L., Picker, J. D., Schaevitz, L. R., Tsai, G., Feng, J., Jiang, Z., Chu, H. C., Basu, A. C., Berger-Sweeney, J. and Coyle, J. T. Phenotypic characterization of mice heterozygous for a null mutation of glutamate carboxypeptidase II. Synapse. 2009. 63, 625–635.

Harrison P.J. The neuropathology of schizophrenia. Brain. 1999. 122:593-624.

Hashemi, R., Bradley, W., Lisanti, C. MRI The Basics (2nd ed.). Philadelphia: Lippincott Williams & Wilkins. 2004.

Heckers S., Konradi C. Hippocampal neurons in schizophrenia. J Neural Transm. 2000. 109:891-905.

Huang H., Akbarian S. GAD1 mRNA Expression and DNA Methylation in Prefrontal Cortex of Subjects with SZ. PLoS ONE 2007.2(8).

Huang, S. A Magnetic Resonance Study of the GCPII$^{+/-}$ Mouse Model. Honors Thesis, Wellesley College, Wellesley, MA. 2012.

Iizuka M., Smith M.M. Functional consequences of histone modifications. Curr Opin Genet Dev. 2003.13: 154-160.

Jenuwein T., Allis CD. Translating the histone code. Science. 2001.293: 1074-1080.

Johnstone E., Frith C.D., Crow T.J., Husband J., Kreel L. Cerebral Ventricular Size and Cognitive Impairment in Chroniz SZ. The Lancet. 1976.308 (7992):924-926.

Kaminsky Z.A., Tang T., Wang S.C., Ptak C., Oh G.H., Wong A.H., Feldcamp L.A., Virtanen C., Halfvarson J., Tysk C., McRae A.F., Visscher P.M., Montgomery G.W., Gottesman I.I., Martin N.G., Petronis A. DNA methylation profiles in monozygotic and dizygotic twins. Nat Genet. 2009.41: 240-245.

Iltis I, Koski DM, Eberly LE, et al. Neurochemical changes in the rat prefrontal cortex following acute phencyclidine treatment: an in vivo localized 1H MRS study. NMR Biomed. 2009. 22:737–744.

Kantrowitz J.T., Javitt D.C. Thinking glutamaterically: changing concepts of schizophrenia based upon changing neurochemical models. Clin Schizophr Relat Psychoses.2010. 4(3):189-200.

Kay S.R., Fizbein A., Opler L.A. Positive and Negative Syndrome Scale. Psychiatric University Hospital Zurich. 2007. 1-4.

Kim, D.K., Rordorf, G., Nemenoff, R.A., Koroshetz, W.J., Bonventre, J.V. Glutamate stably enhances the activity of two cytosolic forms of phospholipase A2 in brain cortical cultures.
Biochemical Journal . 1995. 310 (1): 83– 90.

Kubicki M., Park H., Westin C.F., Nestor P.G., Mulkern R.V., Maier S.E., Niznikiewics., Connor E.E., Levitt J.J., Frumin M., Kikinis R., Jolesz F.A., McCarley R.W., Shenton M.E. DTI and MTR abnormalities in schizophrenia: Analysis of white matter integrity. Neuroimage.2005. 26(4):1109-1118.

Kubicki M., Westin C.F., Maier S.E., Frumin M., Nestor P.G., Salisbury D.F., Kikinis R., Jolezs F.A., McCarley R.W., Shenton M.E. Uncinate fasciculus findings in SZ: A magnetic resonance diffusion tensor imaging study. Am J Psychiatry. 2002.159:813-820.

Lawrie, S. M., Buechel, C., Whalley, H. C., Frith, C. D., Friston, K. J., and Johnstone, E. C. Reduced fron- totemporal functional connectivity in SZ associated with auditory hallucinations. Biol. Psychiatry.2002.51, 1008–1011.

Le Bihan D., Mangin J.F., Poupon C., Clark C.A., Pappata S., Molko N., Chabriat H. Diffusion Tensor Imaging: Concepts and Applications. Journal of Magnetic Resonance Imaging.2001.13: 543-546.

Leung A., Chue P. Sex differences in schizophrenia, a review of the literature. Acta Psychiatra Scandinavica. 2000. 101: 3-38.

Levitt, J. J., McCarley, R. W., Nestor, P. G., Petrescu, C., Donnino, R., Hirayasu, Y., Kikinis, R., Jolesz, F. A., and Shenton, M. E. Quantitative volumetric MRI study of the cerebellum and vermis in schizophrenia: clinical and cognitive correlates, Am J Psychiatry. 1999. 156: 1105–1107.

Lewis D.A., Levitt P. SZ as a Disorder of Neurodevelopment. Annu. Rev. Neurosci. 2002. 25, 409-432.

Leung A., Chue P. Sex differences in schizophrenia, a review of the literature. Acta Psychiatr Scand. 2000. 101: 3-38.

Liang, M., Zhou, Y., Jiang, T., Liu, Z., Tian, L., Liu, H., and Hao, Y. Widespread functional disconnectivity in SZ with resting-state functional magnetic resonance imaging. Neuroreport. 2006.17, 209–213.

Lorrain DS, Baccei CS et al. Effects of ketamine and N-methyl-D-aspartate on glutamate and dopamine release in the rat prefrontal cortex: modulation by a group II| selective metabotropic glutamate receptor agonist LY379268. Neuroscience. 2003.117: 697–706.

Lutkenhoff E.S., Erp T.G.V., Thomas M.A., Therman S., Manninen M., Huttunen M.O., Kaprio J., Lo¨nqvist J., O'Neill J., Cannon T.D. Proton MRS in twin pairs discordant for schizophrenia. Molecular Psychiatry. 2010. 15:308-318.
Maas.L.C. Diffusion tensor imaging: Basic principles and emerging clinical applications. Supplement to Applied Radiology. 2003. 49-57.

Maier, M., Ron, M. A., Barker, G. J., and Tofts, P. S.Proton magnetic resonance spectroscopy: an in vivo method of estimating hippocampal neuronal depletion in schizophrenia, Psychol. Med.1995. 25:1201.

Marona-Lewicka D., Nichols C.D., Nichols D.E. An Animal Model of SZ Based on Chronic LSD Administration: Old Idea, New Results. Neuropharmacology.2011.61 (3):503-512.

Marsman A., Martijn P.vdH., Klomp D.W.J., Kahn S.R., Luijten, P.R., Hulshoff Pol, H.E. Glutamate in SZ: A focused Review and Meta-Analysis of ^{1}H-MRS studies. SZ Bulletin. 2013.1(9):120-129.

Mayer C., Acosta-Martinez M., Dubois S.L., Wolfe A., Radovick S., Boehm U., Levine J.E. Timing and completion of puberty in female mice depend on estrogen receptor α-signaling in kisspeptin neurons. PNAS. 2010. 107(52): 22693-22698.

Milkevitch M., Shim H., Pilatus U., Pickup S., Wherle J.P., Samid D., Poptani H., Glickson J.D., Delikatny J.E. Increase in NMR-visible lipid and glycerophosphocholine during phenylbutyrate-induced apoptosis in human prostate cancer cells. Biochimica et Biphysica Acta. 20045. 1734:1-12.

Moghaddam B, Adams B, Verma A, Daly D. Activation of glutamatergic neurotransmission by ketamine: a novel step in the pathway from NMDA receptor blockade to dopaminergic and cognitive disruptions associated with the prefrontal cortex. J Neurosci 1997.17:2921–2927.

Moghaddam B., Javitt D. From Revolution to Evolution: The Glutamate Hypothesis of Schizophrenia and its Implication for Treatment. Neuropsychopharmacology. 2012. 37:4-15.

Mohn A.R., Gainetdinoc R.R., Caron M.G., Koller B.H. Mice with Reduced NMDA Receptor Expression Display Behaviors Related to Schizophrenia. Cell. 1999. 98: 427-436.

Morris B.J., Cochran S.M., Pratt J.A. PCP: from pharmacology to modeling SZ. Current Opinion in Pharmacology. 2005.5: 101-106.

Mu, W. Assessment of the Neuroanatomy and Neurochemistry GCPII+/- Mouse Model with Magnetic Resonance Imaging and Spectroscopy. Honors Thesis, Wellesley College, Wellesley,MA. 2011.

Nakazawa K., Zsiros V., Jiang Z., Nakao K., Kolata S., Zhang S., Belforte J.E. GABAergic interneuron origin of schizophrenia pathophysiology. Neuropharmacology. 2012. 62(3):1574-1583.

Ongur, D., Prescot, A. P., Jensen, J. E., Cohen, B. M., and Renshaw, P. F. Creatine abnormalities in schizophrenia and bipolar disorder, Psychiatry Research-Neuroimaging.2009.172:44–48.

Organization, W. International Statistical Classifiication of Diseases and Health Problems. Geneva: World Health Organization. 2004.

Os J.V., Rutten B.PF., Poulton R. Gene-Environment Interactions in SZ: Review of Epidemiological Findings and Future Directions. SZ Bulletin. 2008. 34(6): 1066-1082.

Paparelli A., Forti M.D., Morrison P.D., Murray R.M. Drug-induced psychosis:how to avoid star gazing in SZ research by looking at more obvious sources of light. Frontiers in Behavioral Neuroscience. 2011. 5(1):1-9.

Paz R.D., Tardito S., Aztori M., Tseng K.Y. Glutamaterfic Dysfunction in Schizophrenia: from basic neuroscience to clinical psychopharmacology. Eur Neuropsychopharmacol. 2008. 18 (11): 773-786.

Powell S.B., Zhou Z., Geyer M.A. Prepulse Inhibition and Genetic Mouse Models of Schizophrenia. Behav Brain Res. 2009. 204 (2): 282-294.

Peterson C.L., Lanel M.A. Histones and histone modifications. Curr Biol. 2004.14: R546-R551.

Reynolds L.M., Cochran S.M., Morris B.J., Pratt J.A., Reynolds G.P. Chronic phencyclidine administration induces schizophrenia-like changes in N-acetylaspartate and N-acetylaspartylglutamate in rat brain. Schizophrenia Research. 2005. 73:147-152.

Rung J.P., Carlsson A., Markinhuhta K.R., Carlsson M.L.(+)-MK-801 induced social withdrawal in rats; a model for negative symptoms of schizophrenia. Progress in Neuro-Psychopharmacology & Biological Psychiatry. 2005. 29: 827-832.

Schaevitz L.R., Picker J.D., Rana J., Kolodny N.H., Shane B., Sweeney J.E.B., Coyle J.T. Glutamate Carboxypeptidase II and Folate Deficiences Result in Reciprocal Protection Against Cognitive and Social Deficits in Mice: Implications for Neurodevelopmental Disorder. Wiley Online Library. 2011, 891—905.

Sandhya, T.L., Ong, W.Y., Horrocks, L.A., Farooqui, A.A. A light and electron microscopic study of cytoplasmic phospholipase A2 and cyclooxygenase-2 in the hippocampus after kainite lesions. Brain Research. 1998. 788 (1– 2):223–231.

Schmahmann JD. From movement to thought: Anatomic substrates of the cerebellar contribution to cognitive processing. Human Brain Mapping.1996.4:174–198.

Schuller-Levis, G. B., and Park, E. Taurine: new implications for an old amino acid, Fems Microbiology Letters.2003.226: 195–202.

Sepulcre J., Masdeu J.C., Sastre-Garriga J., Goni J., Velez-de-Mendizabal N., Duque B., Pastor M.A., Bejarano B., Villoslada P. Mapping the brain pathways of declarative verbal memory: Evidence from white matter lesions in the living human brain.NeuroImage.2008. 42 (3):1237-1243.

Sharma R.P., Grayson D.R., Galvin D.P.. Histone Deacetylase 1 expression is increased in the prefrontal cortex of SZ subjects; analysis of the National Brain Databank microarray collection. Schizophr Res. 2008; 98 (1-3): 111-117.

Shenton M.E., Whitford T.J., Kubicki M. Structural neuroimaging in SZ: from methods to insights to treatments. Dialogues in Clinical Neuroscience. 12(3): 317-332.

Shergill SS, Kanaan RA, Chitnis XA, O'Daly O, Jones DK, Frangou S, et al. A diffusion tensor imaging study of fasciculi in schizophrenia. American Journal of Psychiatry 2007.164:467-473.

Shirayama, Y., Obata, T., Matsuzawa, D., Nonaka, H., Kanazawa, Y., Yoshitome, E., Ikehira, H.,Hashimoto, K., and Iyo, M. Specific metabolites in the medial prefrontal cortex are
associated with the neurocognitive deficits in schizophrenia: A preliminary study, Neuroimage.2010.49:2783–2790.

Sigmundsson, T., Maier, M., Toone, B. K., Williams, S. C. R., Simmons, A., Greenwood, K., and Ron, M. A. Frontal lobe N-acetylaspartate correlates with psychopathology in schizophrenia: a proton magnetic resonance spectroscopy study, Schizophrenia Research.2003.64: 63–71.

Slusher BS, Vornov JJ, Thomas AG, et al. Selective inhibition of NAALADase, which converts NAAG to glutamate, reduces ischemic brain injury. Nat Med. 1999.5(12):1396–402.

Stahl, S.M. Beyond the Dopamine Hypothesis to the NMDA Glutamate Receptor Hypofunction Hypothesis of SZ. Trends in Psychopharmacology. 2007, 12(4): 265-268.

Theberge, J., Al-Semaan, Y., Williamson, P.C., Menon, R.S., Neufeld, R.W., Rajakumar, N., Schaefer, B., Densmore, M., Drost, D.J. Glutamate and glutamine in the anterior cingulate and thalamus of medicated patients with chronic schizophrenia and healthy comparison subjects measured with 4.0-T proton MRS. The American Journalof Psychiatry. 2003. 160 (12), 2231–2233.

Tiffany CW, Cai NS, Rojas C, Slusher BS. Binding of the glutamate carboxypeptidase II (NAALADase) inhibitor 2-PMPA to rat brain membranes. Eur J Pharmacol. 2001. 427(2):91–6.

Uhlhaas PJ, Singer W. Abnormal neural oscillations and synchrony in schizophrenia. Nat Rev Neurosci. 2010.11:100–113.

Velakoulis D, Pantelis C, McGorry PD *et al*. Smaller hippocampi in chronic schizophrenia and first-episode schizophrenia and affective psychoses: a high resolution magnetic resonance imaging study. Archives of General Psychiatry.1999. 56:133–141.

Wang Y., Fischle W., Cheung W., Jacob S., Khorasanizadeh S., Allis C.D. Beyond the double helix: writing and reading the histone code. Novartis Found Symp. 2004; 259: 3-17.

Yerby B.L. Localized ^{1}H Magnetic Resonance Spectroscopy of Brain Metabolites in the Study of the Murine Model for Rett Syndrome. Honors Thesis, Wellesley College, Wellesley, MA. 2005.

Appendix A. Behavioral Experiments

This is a guide for the set-up, execution and analysis of behavioral testing on mice. Male and female mice are tested between postnatal day (PND) 114 and 117. Testing is conducted in room L336 in the Wellesley College Animal Facilities. The social paradigm assesses the social preference of test mice by determining how much time they choose to spend in a space with a stranger mouse vs. an empty space. The behavioral apparatus has two side chambers, one of which will contain the stranger mouse. Experimenters are blind to the genotype of the mouse during testing. Anticipating the effect that the side of the stranger mouse can have on social preference, stranger chamber assignment should be requested from Pat Carey to verify that each side is equally assessed throughout all tests.

1. Setup of the paradigm necessitates the use of a large cardboard box to enclose Plexiglas apparatus. Pictures below display Plexiglass apparatus alone however.
2. Once the Plexiglas apparatus is placed inside the cardboard box, make sure to wipe down all surfaces with PPE Cleaning Towelettes (Fisherbrand).
    - Check that vertical doors are blocking openings in central chamber and that cages are inverted with empty glass bottles placed on top as weights (picture below).

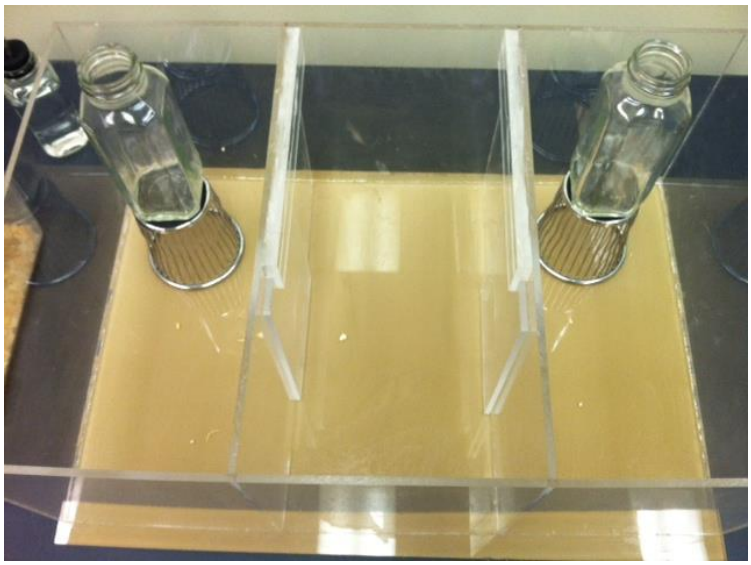

3. Set up of the Sony™ DCR-SX85 digital video camera video and tripod. Both camera and tripod should be located in Kolodny lab room, SCI 2XX.

    ○ Adjust the DYNEX™ DX-TRP60 tripod to its maximum height and click in the video camera.

    ○ Make sure that the camera is charged and the visual field encompasses whole apparatus.

4. Bring the cages housing test mice and stranger mice into room. Prepare an empty cage with shavings and metal cover as intermittent housing between phases of test. Prepare record in lab notebook denoting mouse number, gender, ear clipping and side of stranger mouse. Write down these identifiers on a piece of paper that will later be videotaped prior to the testing session (example below).

Mouse # 400 male bk1 Stranger (L)

5. *Habituation phase* Set stopwatch to ten minutes and place test mouse in central chamber, record time period.

6. After ten minutes remove test mouse and place into intermittent empty cage.
7. Free one of the wire cages from the glass weight and place stranger mouse inside. Then flip the cage down onto the platform of its corresponding side chamber, returning glass bottle weight.
8. Remove sliding doors; hit ‘record’ on camera and videotape paper with identifiers to note which mouse is being tested and experimental conditions.

9. *Sociability phase* Now return the test mouse into test chamber and note time, allow for ten minutes of exploration.

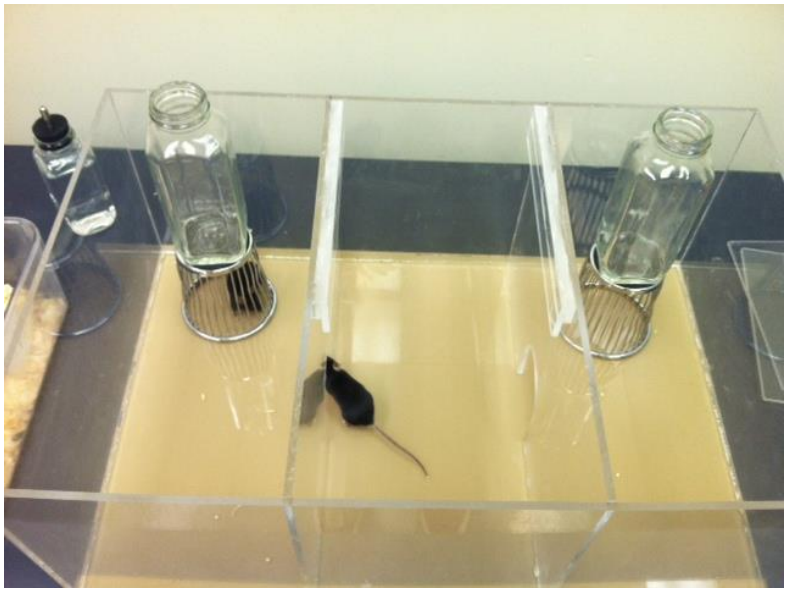

10. Hit ‘stop’ on camera and return test mouse to home cage. Replace sliding doors, remove glass bottle weight and bring wire cage containing stranger mouse to its corresponding cage and allow for mouse to climb out.

*Wipe down surface in between test mice but **not** in between habituation (number 5) and sociability phase (number 7) for each mouse. Mice will usually urinate and defecate in central chamber and therefore cleaning this might negate their familiarity with the space.*

- ❖ Analysis of Behavioral data
    - Digital recording is stored on camera’s internal memory and should be transferred via USB cable to lab computer. File sizes are too large to

be burnt onto current DVDs and therefore should be backed up onto external hard drive.

- Object of analysis is to document amount of time mouse spends in each chamber. Time in central chamber is not important for data analysis but ensures accurate recording. Sample table of data is provided below.

Left Chamber	Center Chamber	Right Chamber *
3.00-4.15	**0.25**-1.00	1.00-1.45
6.00-7.30	1.45-3.00	8.40-9.50
10.18-**10.25**	4.15-6.00	
	7.30-8.40	
	9.50-10.18	

- Bolded numbers are to show that only the first ten minutes of video should be analyzed. First timestamp should correspond to moment test mouse is placed in center chamber. Asterisk (*) denotes which chamber stranger mouse is in.
- Calculate the total time each mouse spent in the stranger chamber* and the empty chamber. Determine the average time mice spent in each chamber for all four experimental groups; Female HET, Female WT, Male HET, Male WT.
- Run Student's T-test within each experimental group separately. Conduct paired one-tailed assuming equal variance for HET mice and a paired two-tailed t-test assuming equal variance for WT mice.

Appendix B. Diffusion Tensor Imaging

This section provides a guide on how to manually shim the magnetic field prior to imaging and the post processing of DTI data. General instructions for running MRI instrument are found elsewhere.

1. Tune and match your sample first. Once probe is placed and ^{1}H cable is connected, go to spectrometer control tool window, click acquire and choose wobble.
2. Now load the SINGLEPULSE_1H scan by going to ParaVision Scan control tool→New Scan→B_Spectroscopy and choosing SINGPULSE_1H scan.
3. To allow for a seamless adjustment over time, edit the number of reps in the scan to 200 by selecting scan→clicking edit method in spectrometer control tool which will bring you to parameter window.
4. Next, load shim file by going to Spectrometer control tool window→Tools→Shim Tool→Load from file→Steph4.
5. Prior to hitting the traffic light icon, increase Tx0 Attenuator value to ~33.9.
6. Scan is now running. To homogenize the magnetic field, you want to adjust the X, Y, Z and Z^2 values. Object of shimming is to obtain a symmetrical water peak and a gradual free induction decay (shown below).
7. Begin by adjusting the Z value to left followed by the Z^2, X and Y. Repeat as necessary.
8. Once shimming is completed, stop the scan and run RARE_Tripilot and RARE_8_bas. Established protocols should be followed for these scans (Mu 2011).

9. Load EPI-diffusion-tensor scan by choosing New Scan and setting Location to B_DIFFUSION.
10. Select scan and go to spectrometer control tool→edit method→ set Echo Time to 33 msec, and the repetition time to 2850 msec on first window.
11. Click on radio button ‘expand’ next to Diffusion and make sure that diffusion experiment is set to DW_Tensor with 30 diffusion directions, 1 diffusion experiment per direction and 5 A0 images. Scroll down to change bandwith value to 786.73 s/mm^2 next to B values per direction.
12. Expand Standard in plane geometry interface and change Field of View (FOV) parameters to 20 mm x 20 mm. Finally expand Standard slice geometry interface and set it to 0.8 mm.
13. Tune and match your sample again by choosing wobble from Acquire drop down menu on spectrometer control tool.
14. Select EPI-diffusion-tensor scan and go to geometry editor  on Scan control window. Load corresponding RARE_Tripilot scan and set number of slices to 19. Make sure that slices cover entire brain on sagittal image and click accept. Now run the scan by hitting the traffic light icon  .

Post-Processing of DTI Data (ParaVision A07_Tools, O8_ImDispProcTool, O9_MPR_DTI_VISU)

15. Dataset obtained from EPI-diffusion-tensor scan must be post processed. Open Image Display window if not already there by going to System Control→Tools→Image Display & Processing.
16. Select scan from window in ParaVision scan control and then from Image Display & Processing, choose the Processing drop down menu. From here click DTI Tensor Reconstruction →All Slices.
17. The reconstructed set of slices should appear as new dataset in scan control menu; if it does not then click scan, and scroll to the scan ID which has one greater third coordinate value. For example, if reconstructing scan 1.5.1, the new dataset would be 1.5.2.
18. The reconstructed dataset contains tensor trace images, Fractional Anisotropy images, A0 images, eigenvalue and eigenvector images.
19. To determine fractional anisotropy values select fractional anisotropy image corresponding to structure of interest on Image Display & Processing window. Next, choose the region of interest ROI tool from the top panel in the window and a ROI tool window should appear.

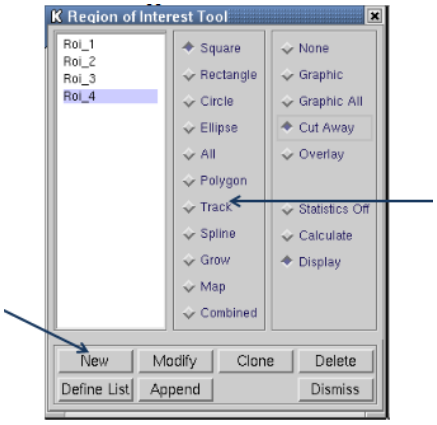

20. Click command button **New** to highlight a tract or bundle within the coronal image. To allow for flexibility, choose the ROI type **Track** and outline the region you would like to analyze. The ROI tool window will expand allowing user to select for desired intensity regions within the traced portion using the sliders ‘Min. Intensity’ and ‘Max. Intensity.

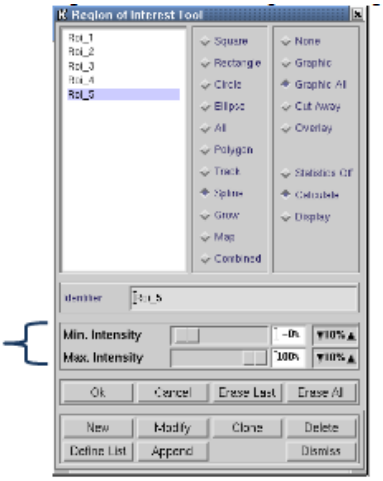

21. On ROI tool click the radio button ‘Display’ which will calculate and display the statistical values associated with that region. The FA value is the mean intensity

value of the source displayed in the statistics and histogram window.

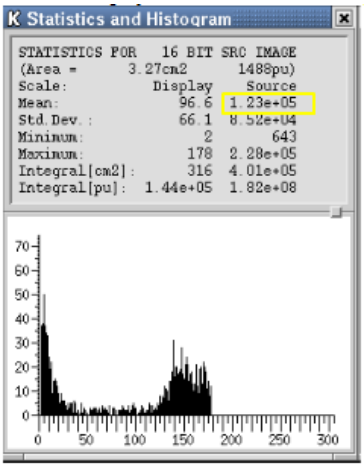

22. To calculate mean diffusivity or the Apparent Diffusion Coefficient (ADC), utilize the Image Sequence Analysis tool from the drop down 'Processing' Menu on the Image Display & Processing window. This should render a main ISA (Image Sequence Analysis) window. Make sure that you are analyzing diffusion tensor trace image.
23. Click New ISA ROI and now position and size the ROI tool over the region you wish to analyze. Click Points only →Pnts & Curves and then Refresh Cur. ROI.

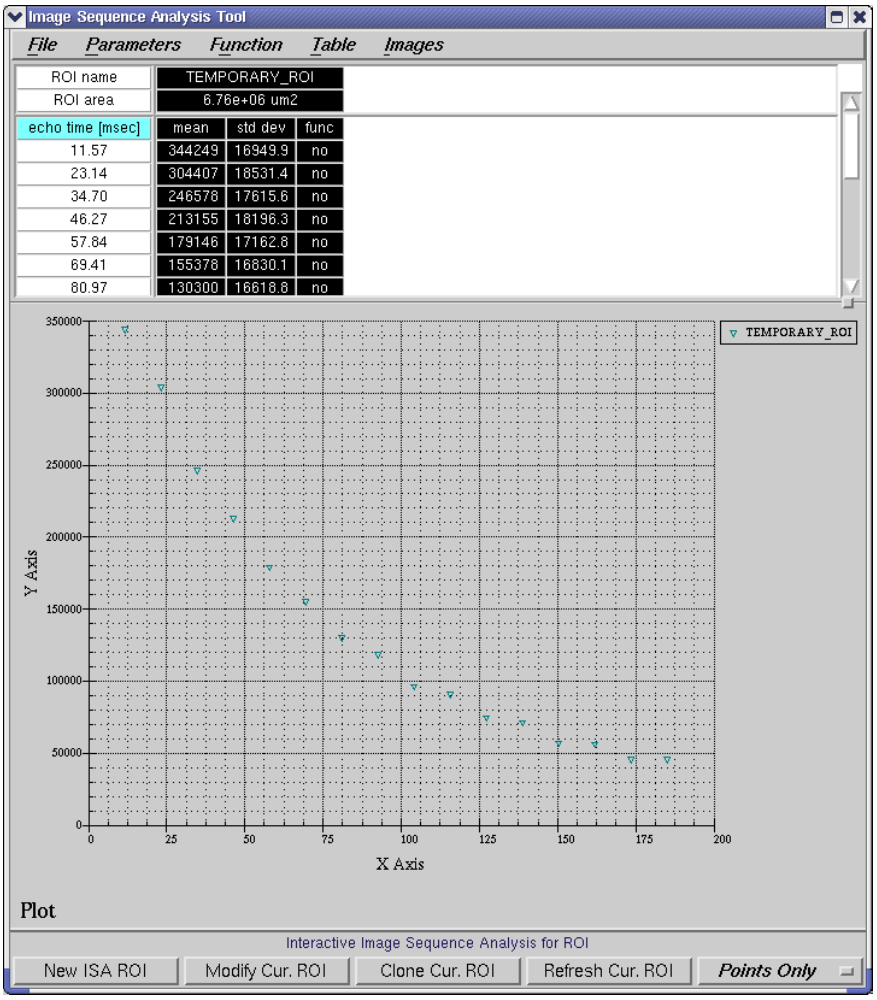

24. Mean diffusivity value will be listed under ‘value’ column corresponding to ‘signal intensity’ row.

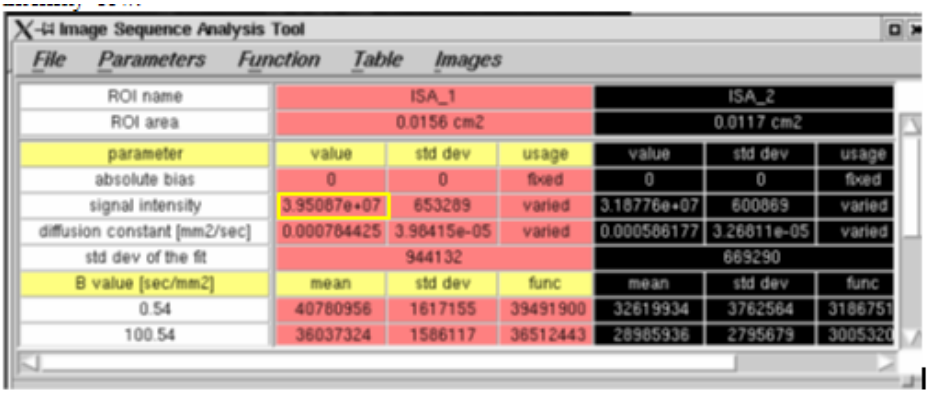

25. To visualize color maps such as below (CIVM), select processed data set (e.g 1.5.2) and go to Processing drop down menu on Image Display & Processing Window→DTI Visualization.

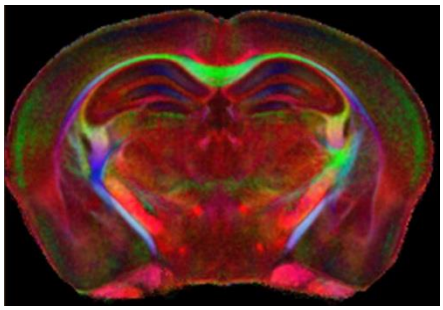

26. Main window interface will now appear.

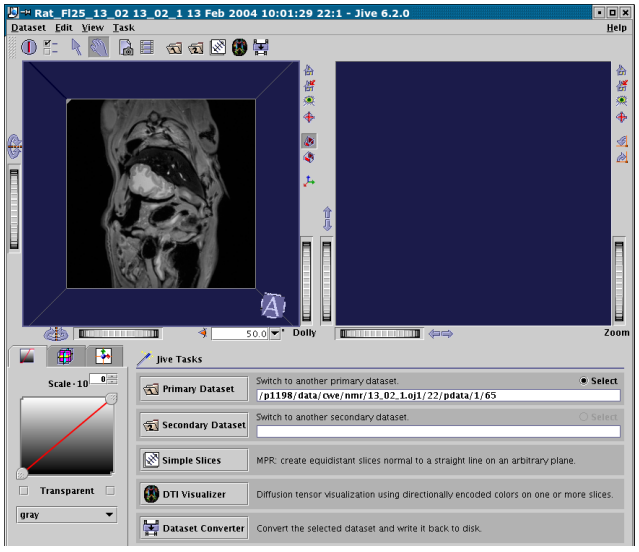

27. In Data Selection panel that is shown below, select A0 in image toolbar under Map and Trace Weighted Image in image toolbar under mask.

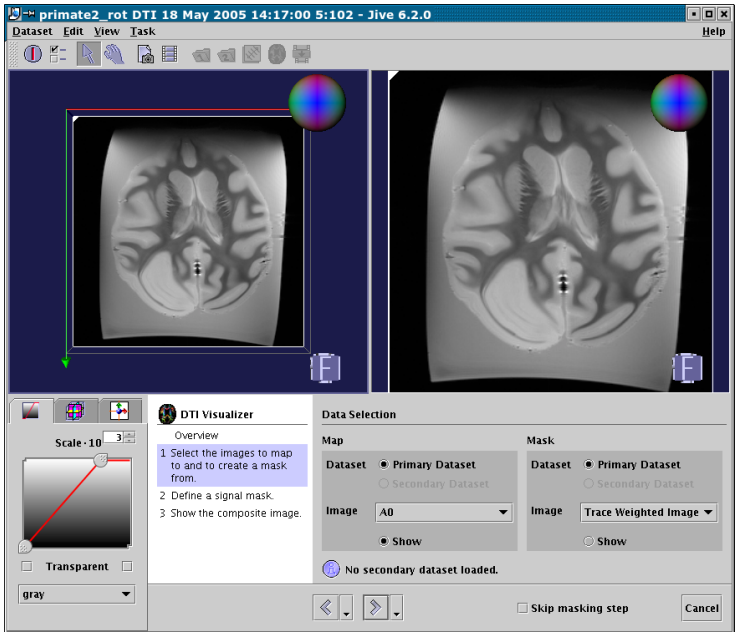

28. Click forward arrow button on bottom of window to move forward to signal mask panel.

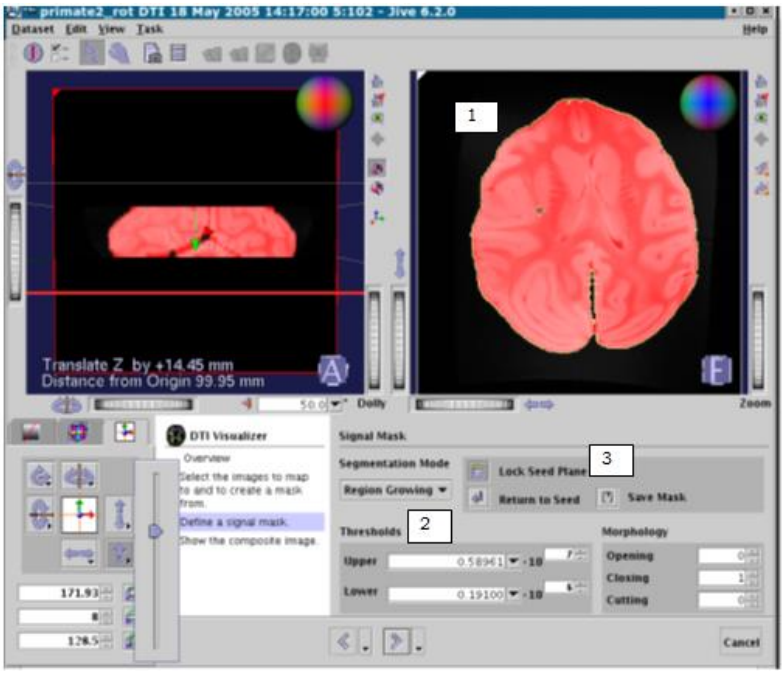

29. Here is where the region within the image to be analyzed is delineated. To do this, click onto the right plane image (1) and adjust the threshold sliders (2) to cover all of brain; this is called setting the seed point. When satisfied, click Lock Seed Plane (3).
30. Next, click forward arrow to display the composite images. The DTI Visualization will display a color coded map in accordance with the three eigenvectors (1[Left→Right] = Green, 2 [Top→Down] = Blue, 3[In→Out] = Red). Different colors thus illustrate different diffusion directions.

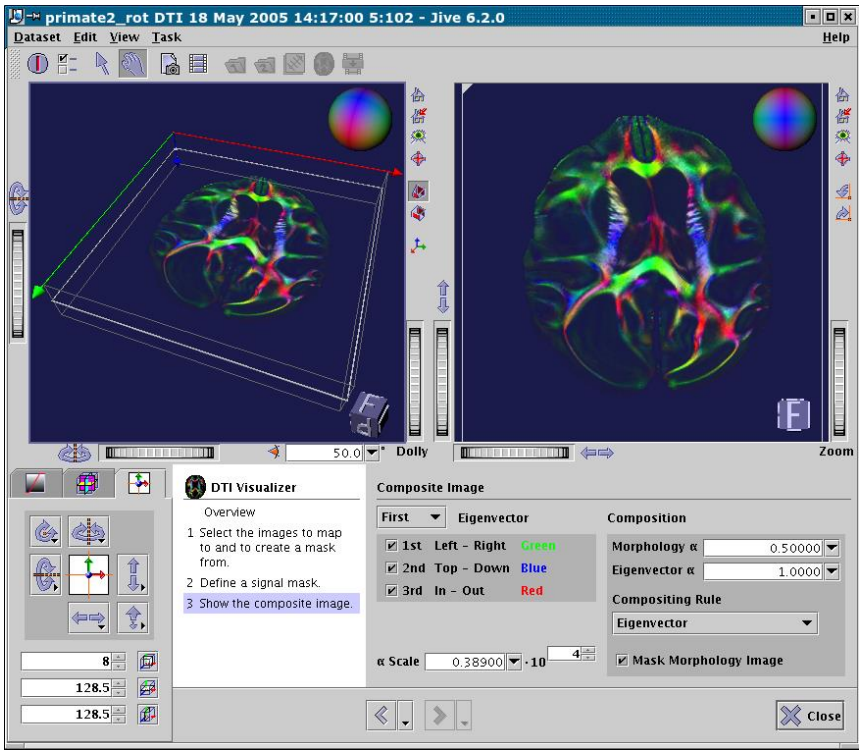

31. Buttons next to Eigenvectors can be selected or unselected in order to allow for custom visualization of each vector.

Appendix C. Stereotactic Neonatal Surgeries

This is a preliminary procedure for stereotactic surgeries on neonatal (postnatal day 1) mice and for the removal of their brains. Surgeries take place in surgery room L342 in the Wellesley College Animal Facilities. Preliminary experiments inject cresyl violet to indicate the success of bilateral injections in practice rounds; final experiments use adeno-associated virus containing HDAC1 cDNA and saline.

1. Make sure to have sufficient levels of isoflurane and cresyl violet prior to set up.
2. Place stereotax on operation table and center neonatal mouse upon platform on base of stereotax.
3. Draw approximately 2 uL of cresyl violet into Hamilton syringe. Then place the syringe in the automatic injector accessory as shown below. Experimenters can preset the volume and this will allow for a steadier more uniform injection.

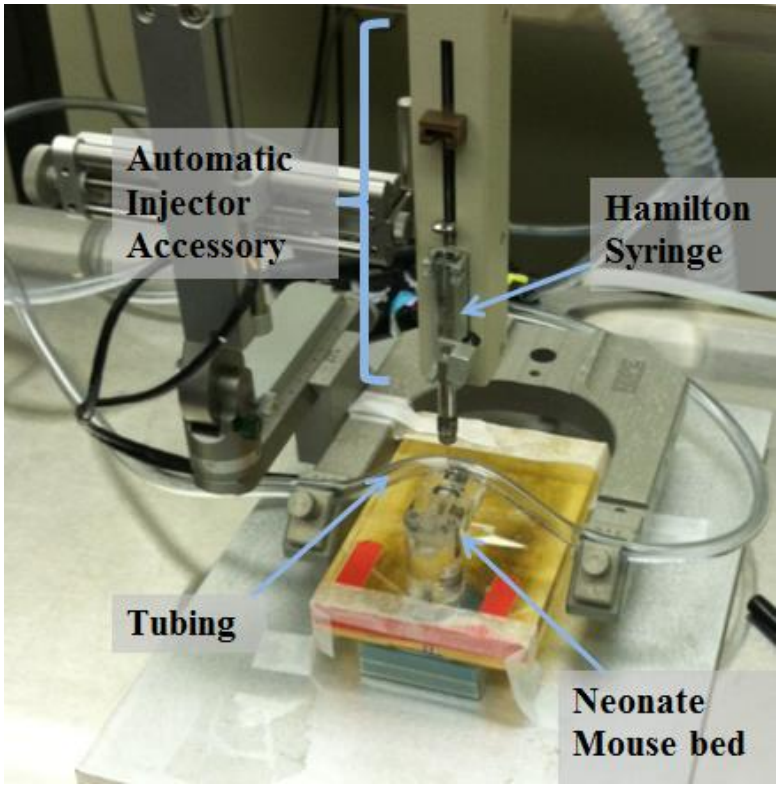

4. Set up isoflurane chamber and valve regulator so that there is one tubing loop from isoflurane chamber to induction chamber via valve regulator to filter, and another loop from isoflurane chamber to stereotax via valve regulator and then to filter .

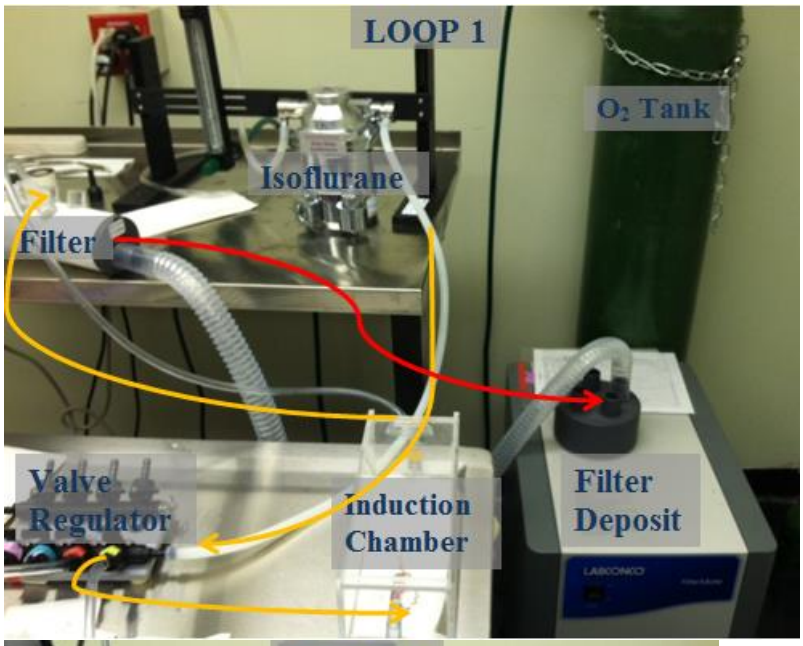

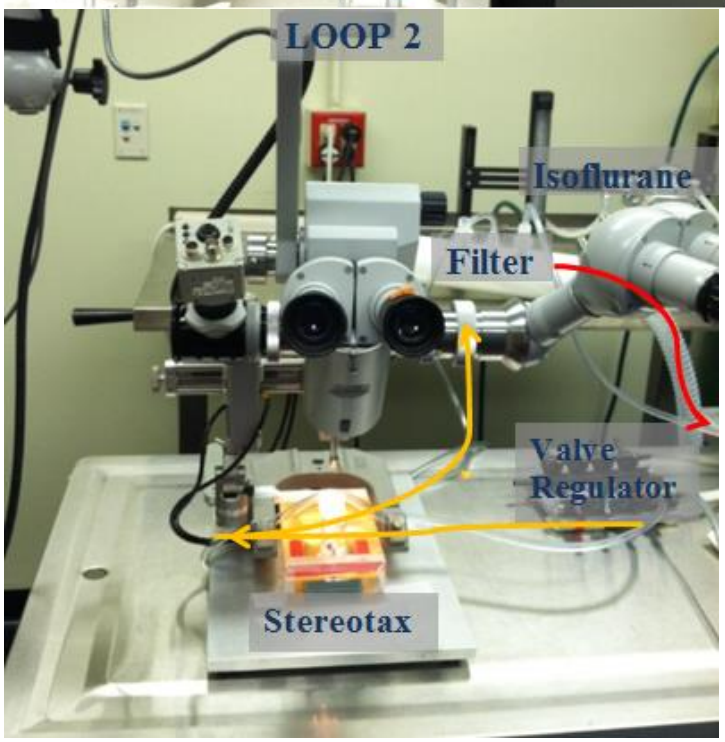

5. Tube in secondary loop has a notch that must be placed over the neonate's nose in order to maintain a steady stream of anesthesia during procedure. The tubing should be placed on anterior portion of mouse bed prior to neonate placement

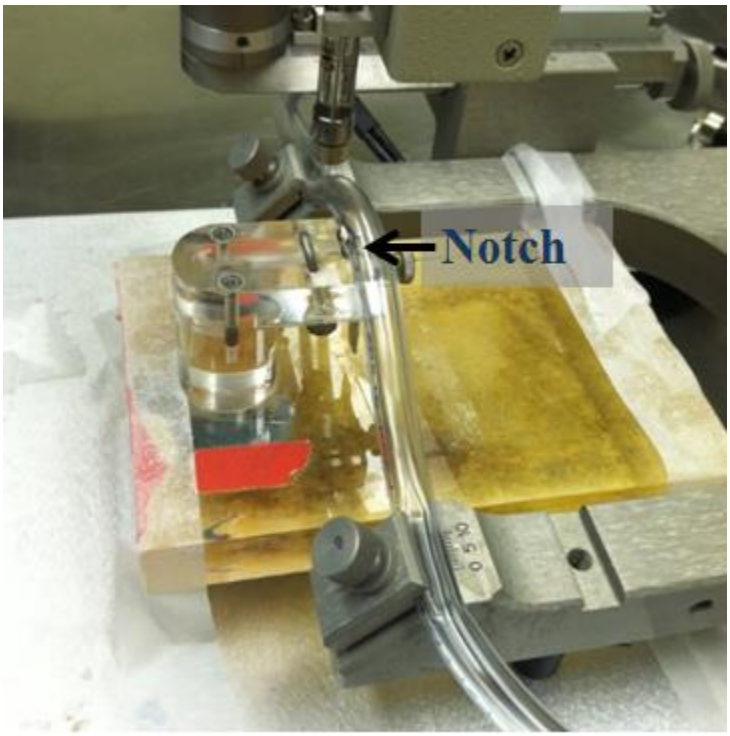

6. Make sure valve for tubing to induction chamber is turned perpendicular to regulator then turn on oxygen tank, set lower valve of regulator to 0.5 to 1 Liters/minute of O_2 and isoflurane dial between 4% and 5%. Place neonatal mouse pup in chamber and wait approximately ten minutes for mouse to fall asleep; pinch pup's foot to confirm.

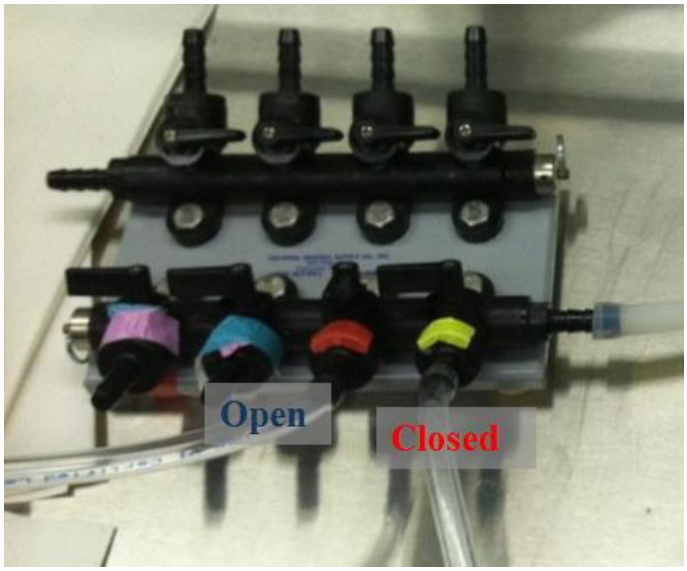

7. Once the mouse is asleep, close valve for induction chamber by making knob parallel; turn valve corresponding to the stereotax perpendicular to regulator to allow for gas flow. Adjust isoflurane flow to 3%.
8. Transfer mouse pup quickly into the mouse bed and make sure its nose fits the notch to sustain anesthesia.

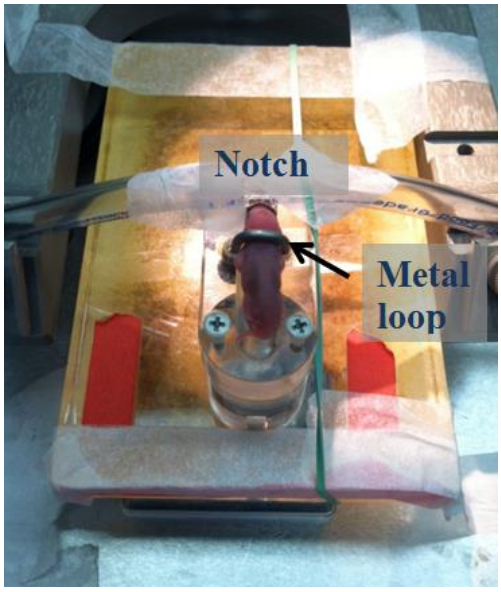

9. Secure the pup flat onto the mouse bed by fitting the metal loop around the neck and pulling down.
10. Once the pup is secured, situate the needle above its head by rotating the upright holder and locking into place with metal knob.

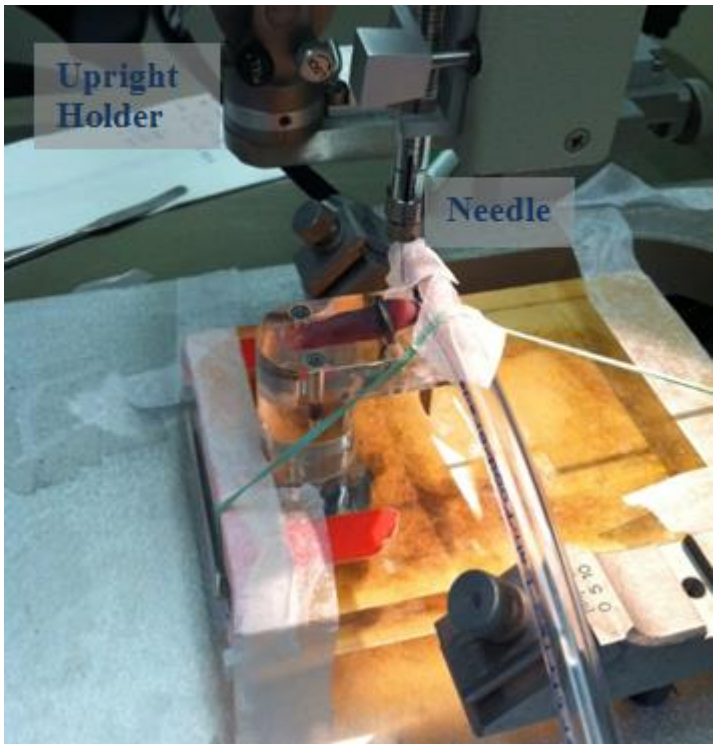

11. The stereotax allows for syringe adjustment in three planes; dorsal/ventral, posterior/anterior and medial/lateral. Adjustments are measured with a vernier scale, so that the syringe can be precisely moved to a set of coordinates relative to bregma, where the sagittal and coronal sutures intersect on the skull (Image borrowed from Li and Daly 2002).

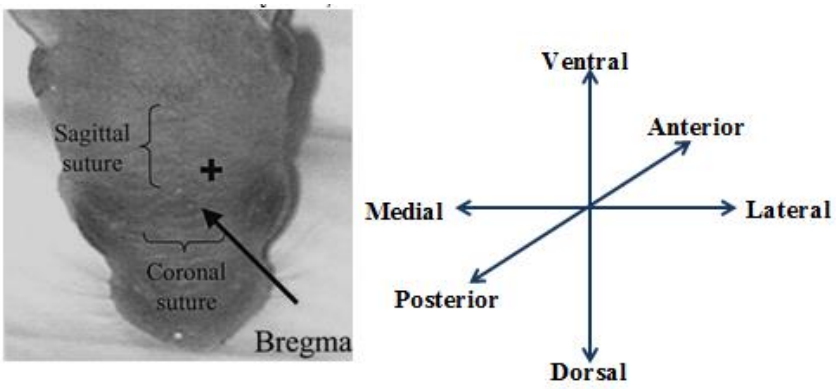

12. The syringe is first aligned on top of bregma and the needle is then brought to the following coordinates with the vernier scale. A/P: +0.75 mm, M/L: ±0.25 mm, D/V -0.75 mm.

Example of coordinate reading on vernier scale of 5.17 cm or 51.7mm.

13. Align syringe with anterior/posterior, medial/lateral coordinates first, and then insert needle through skull to proper depth as given.

14. Once syringe is inside, inject cresyl violet by lightly tapping on plunger. In this case, the volume injected is not significant; however in future experiments, automatic injector will be used and injection will occur over a 2 minute period. Following injection, wait two minutes before slowly lifting the syringe out of skull by increasing dorsal/ventral coordinate value. Same procedure is done on both sides of bregma.

    Brain removal conducted as preliminary test for proper coordinates.

15. Once the injections are completed, pups are decapitated using surgery scissors (a,b). Reference photos borrowed from Beaudoin et al. 2012.

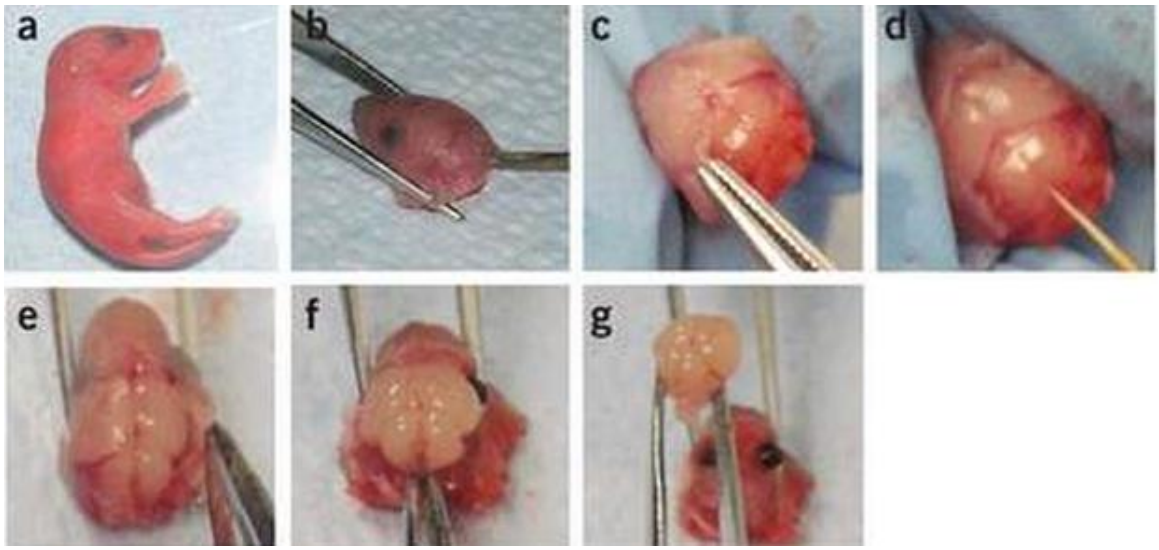

16. A longitudinal incision bisecting the skull is then produced and tweezers are used to peel the skull to the sides of the head (b,c,d). The incision should start at back end of head so that one of scissor blades can easily be passed under the skull tissue (b).

17. A spatula should then be passed along the outer perimeter of the brain to carve out and separate it from the base of the skull.
18. Once brain is free, transfer it to non-stick surface and use a blade to cut through the interhemispheric fissure (image below of Adult mouse brain borrowed from Airey and Williams 2001).

19. Confirm injection of dye by examining cingulate cortex using mouse atlas for guidance; Allen Reference Atlas for mouse, brain of PND 56 mouse shown.